sck cen

Registered Office
Herrmann-Debrouxlaan 40
1160 Brussel – Belgium

Foundation of Public Utility
VAT BE 406.568.867

Research Centres
Boeretang 200
2400 Mol – Belgium

Chemin du Cyclotron 6
1348 Ottignies-Louvain-la-Neuve – Belgium

Reference N°	Creation Date	
SCK CEN/46355212	2023-01-26	
Alternative Reference N°	Revision	Version
N/A	1.0	30
ISC	Revision Status	
Public	Approved	

ER-1008 Sorption of Sn(IV) onto pure clay minerals and Boom Clay

Authors*
Delphine Durce

Review information since previous revision*		
Name	**Outcome**	**Date**
Liesbeth Van Laer	Reviewed	2023-01-26
Lian Wang	Reviewed	2023-01-26

Approval information for current revision*		
Name	**Outcome**	**Date**
Norbert Maes	Approved	2023-01-26
Elke Jacops	Approved	2023-01-27

Change log*				
Revision	**Version**	**Status**	**Date**	**Description of change**
1.0	30	Approved	2023-01-26	

**This automatically generated cover page shows references and document information as were available in the Alexandria document management system on 2023-01-27. Please refer to Alexandria for current and complete metadata, or to the document contents and/or author for additional information.*

ISC motivation
ISC was automatically assigned.

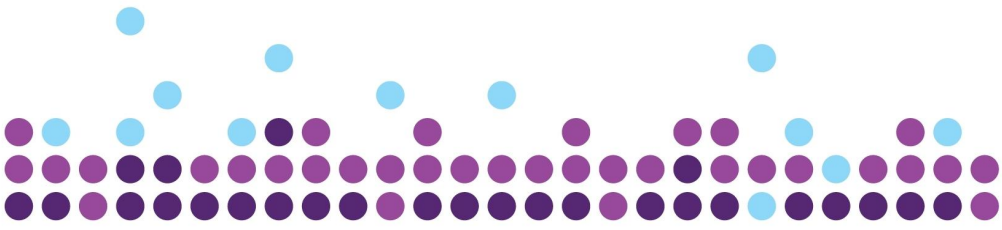

ER-1008

Sorption of Sn(IV) onto pure clay minerals and Boom Clay

Authors: Delphine Durce, Liesbeth Van Laer, Sonia Salah, Lian Wang, Dorien Verhaegen and Norbert Maes

Contract name: SCK/ON PPS MIG, T3-1 Finish Sn sorption
Contract number: CO-90-18-4987-00
Publication date: 2023-01-27

SCK CEN/46355212 Rev. 1.0

sck cen

Exploring
a better tomorrow

Registered Office:
Avenue Herrmann Debroux 40 - 1160 Brussel – Belgium

Research Centres:
Boeretang 200 - 2400 Mol - Belgium
Chemin du Cyclotron 6 - 1348 Ottignies-Louvain-la-Neuve - Belgium

www.sckcen.be

SCK CEN/46355212 Rev. 1.0

Table of content

Abstract

^{126}Sn is a long-lived fission product and it is important to assess Sn sorption onto Boom Clay (BC), which is under investigation in Belgium as a potential host rock for deep geological nuclear waste repository. To better understand Sn(IV) sorption onto the clay minerals constituting BC, sorption of Sn(IV) was here investigated on Illite du Puy (IdP) and montmorillonite STx-1b in various conditions representative of potential repository conditions in BC: $NaClO_4$ 0.017 M in presence or absence of isolated BC dissolved organic matter (DOM), $NaHCO_3$ 0.015 M and Synthetic Seawater (SSW). Sorption edges were acquired from pH 3 to 12 and isotherms were acquired at pH ~8.4 at different Sn(IV) concentrations. Sn(IV) strongly sorbed on IdP and STx-1b over the full range of the pHs and concentrations investigated (log R_d ranging between 4.2 and 5.6 at pH ~8.4). The data obtained on STx-1b suffered from the influence of the used experimental solid/liquid ratio which complicated their interpretation. In the presence of carbonates, Sn(IV) sorption on IdP was slightly decreased (≤ 0.3 log units), highlighting the Sn(IV)–carbonate complexation. The effect of carbonate on Sn(IV) sorption on STx-1b was less clear. The presence of DOM reduced the Sn(IV) sorption on both clays (~0.5 log units on IdP for 4.5 mgC/L), confirming the strong complexation of Sn(IV) with DOM. The increase of salinity seemed to slightly decrease the Sn(IV) sorption on IdP (0.2 log units), but this result was not confirmed on STx-1b. The results obtained on IdP were modelled with the 2-site protolysis non-electrostatic surface complexation model. The surface complexation constants and aqueous complexation constants with carbonate and DOM were optimized to describe the experimental data. The applicability of the component additivity approach (CAA) was also tested to describe the experimental Sn(IV) sorption isotherm acquired on BC in BC pore water. The CAA provided a rough estimation of Sn(IV) sorption onto BC, but did not allow an accurate prediction highlighting the high sensitivity of the model to the Sn(IV)-DOM complexation.

This report is produced as deliverable of the Project Agreement 21-SCK-D_MIG-05-3-1 (Sn sorption on clay; SCK CEN ref CO-90-18-4987-34) of the 2021-2025 framework contract 'Public Public Partnership' (SCK CEN ref CO-90-18-4987-00, ONDRAF/NIRAS ref CCHO 2020-0419/00/00).

Keywords

Organic Matter, Complexation, Sorption, Boom Clay , Tin, thermodynamic sorption model

1 Introduction

^{126}Sn is found in radioactive waste and assessing its mobility through potential host rocks for deep geological disposal is a needed step to complete a safety assessment. Yet, data on Sn behaviour under repository conditions are scarce and not well constrained. In most environmental conditions and more specifically in most repository conditions, Sn is expected to be mainly present as Sn(IV). The sorption of radionuclides (RNs) on the potential clay-rich host rocks considered for nuclear waste repository is dominated by the 2:1 clay minerals. However, only few studies were focussed on the sorption of Sn(IV) onto those clay minerals or on the clay host rocks themselves.
The work presented in this report has three main objectives. On the one hand, it aims at gaining more insight into the sorption behaviour of Sn(IV) onto 2:1 clay minerals with the consideration of the effect of various environmental factors (organic and inorganic ligands and ionic strength) relevant within the context of waste disposal and more specifically waste disposal into Boom Clay (BC). The second objective is to develop and/or test a thermodynamic sorption model to describe the Sn(IV) sorption behaviour onto the 2:1 clay minerals under the investigated conditions.
In a last objective, this work also intends to serve as a demonstration case to assess the validity of the experimental and modelling methodology in predicting sorption of relevant radionuclides on natural systems, i.e. argillaceous host rocks, using a component additivity approach built on the results obtained on simple systems, i.e. pure clay minerals.

The first objective is tackled by the acquisition of Sn(IV) sorption edges and isotherms on both Illite du Puy (IdP) and montmorillonite STx-1b in various conditions representative of potential repository conditions in BC: $NaClO_4$ 0.017 M in presence or absence of isolated BC dissolved organic matter (DOM), $NaHCO_3$ 0.015 M and Synthetic Seawater (SSW). In the safety study for a nuclear waste repository in BC, several scenarios need to be considered. As a reference case, disposal under present-day BC conditions found at the Mol site has been extensively investigated. The composition of the pore water (De Craen et al., 2004; Durce et al., 2015) under these conditions is close to a 0.015 M $NaHCO_3$ solution of pH ~8.4 with a DOM concentration measured by Durce et al. (2015) varying from 60 to 270 mgC/L along the BC formation. The first three conditions investigated in the present work aim at a better understanding of the sorption of Sn(IV) in present day BC conditions at the Mol site notably by studying the role of carbonates and DOM. BC extends over the Campine Basin in north-eastern Belgium and some locations contain a more saline pore water displaying seawater signature (De Craen et al., 2006). At the Mol site, a gradual change of the pore water composition from the current $NaHCO_3$-type to a NaCl-type of water (DeCraen et al., 2012) due to marine inundation is also a considered as a possible long term scenario. In agreement with the work of Durce et al. (2020b), Van Laer (2019) and Van Laer et al. (2020), SSW is here used to investigate the scenario of increased salinity on the sorption of Sn(IV).

The experimental data are first modelled using the 2SPNE SC/CE model developed by Bradbury and Baeyens (1997) to describe the sorption of cations on Montmorillonite SWy and further extended to Illite du Puy (Bradbury and Baeyens, 2009). This model is largely used to describe sorption of radionuclides on montmorillonite and illite and is accepted as one of the thermodynamic sorption models (Payne et al., 2013). As discussed by Bradbury and Baeyens (2005b), Sn(IV) is expected to hydrolyse from low pH and the contribution of cation exchange in its sorption can be assumed negligible. The 2SPNE SC/CE can therefore in most conditions be reduced to a 2SPNE SC model in which the contribution of the cation exchange is neglected. With the 2SPNE SC(/CE) model as basis, the thermodynamic sorption model is extended and optimized to describe the Sn(IV) taking into account the investigated environmental factors.

The last objective is tackled by investigating the sorption of Sn(IV) onto Boom clay in present day BC conditions at the Mol site. The determination of the relevant constants needed to describe the Sn sorption on the pure clay minerals are implemented within a component additivity approach and the resulting model is tested against the experimental results.

This report was written in parallel to a peer-reviewed publication, Durce et al. (2022), and some parts of the text were directly adapted from the publication.

2 Materials and Method

2.1 Pure Clay minerals and Boom Clay

The main objective of this work was to quantify the interaction of Sn(IV) with pure clay minerals to set the bases of the component additive (CA) modelling approach and to further describe Sn(IV) sorption onto Boom Clay or other relevant clay-rich environments. As described by Marques Fernandes et al. (2015), the CA approach referred also to as 'bottom-up' approach is a predictive modelling which combines in an additive way the sorption properties of each individual minerals constituting the natural system accounting for their relative concentration. In case some minerals strongly dominate the sorption, the CA approach can be simplified and account for only these minerals. The main RN sorbing clay minerals in Boom Clay being 2:1 clay minerals as illite and smectite, it was chosen to focus here on the sorption of Sn(IV) onto Illite du Puy and Montmorillonite STx1-b.
In addition to pure clay minerals, sorption of Sn(IV) was also investigated onto Boom Clay to evaluate the validity/applicability of the CA model.

2.1.1 Illite du Puy (IdP)

Various types of illite can be found on the market. Studies focused on the sorption of RNs generally make use of the Silver Hill illite or the Illite du Puy and both types were used in SCK CEN in previous works (Van Laer et al., 2016). Yet, the most recent studies performed within SCK CEN and within the context of the CatClay European project (Altmann et al., 2015) were performed on Illite du Puy and to be consistent with these studies, it was chosen to work here with the same batch of IdP as used in the CatClay project.
The Illite du Puy originates from the clay-rich Puy-en-Velay Formation. As mentioned in Altmann et al. (2015), the Illite du Puy also contains background impurities such as carbonates, feldspars and quartz. As a consequence, the illite batch was purified using a multistep process and saturated in sodium (Na) using the method of Baeyens and Bradbury (1997) and Bradbury and Baeyens (2009). The obtained high purity Na-form Illite du Puy was used in the following experiments and its mean structural formula is assumed to be $Na_{0.08}K_{0.69}Ca_{0.06}(Si_{3.51}Al_{0.49})(Al_{1.20}Mg_{0.39}Fe^{3+}_{0.36})O_{10}(OH)_2$ as reported by Altmann et al. (2015). Various characterizations of the purified IdP were performed within the framework of CatClay and for more information we refer the reader to Altmann et al. (2015).

2.1.2 Montmorillonite STx1-b

Texas montmorillonite is a Ca-rich source clay montmorillonite containing a low amount of structural iron (Fe). It is today the main source of montmorillonite, the commonly used Wyoming montmorillonite (SWy-1) being depleted. Two Texas montmorillonite sources existed, the STx-1a and the STx-1b. In the works reported in literature and making use of the Texas montmorillonite it is not always mentioned which source was used and only the general denomination STx-1 is used. However, as reported by Castellini et al. (2017) STx-1a is frequently cited as STx-1 and we can assume that most of the works mentioning STx-1 refer to STx-1a, at least until STx-1a was out of stock and was replaced with STx-1b (at least from 2017 (Castellini et al., 2017)).
According to Castellini et al. (2017), STx-1a and STx-1b share many basic chemical and mineralogical characteristics, but some minor differences exist that can affect applications. It is therefore important to be cautious when comparing data acquired on STx-1a with data acquired on STx-1b and to avoid as much as possible mixing properties of the two sources (CEC, mineralogy…).

One of the characteristics of the Texas montmorillonite is its low content of structural iron with an Fe_2O_3 content of 0.5-0.9 wt% for the STx-1b (Castellini et al., 2017; Soltermann et al., 2014a) in comparison to the 2.8-2.9 wt% of the widely used Wyoming montmorillonite (SWy-1) (Soltermann et al., 2014a). It has the following published (Castellini et al., 2017) structural formula $^{[4]}(Si_{7.753}Al_{0.247})\ ^{[6]}(Al_{3.281}Mg_{0.558}Fe_{0.136}Ti_{0.024}Mn_{0.002})\ ^{[12]}(Ca_{0.341}Na_{0.039}K_{0.061})O_{20}(OH)_4$. More information of the STx-1b properties can be found in Castellini et al. (2017).

As mentioned by Bradbury and Baeyens (2017), commercially available montmorillonite contains significant levels of background impurities potentially influencing its sorption properties. A conditioning procedure to remove these background metal impurities, soluble salts and sparingly soluble minerals was developed based on various protocols reported in the literature and applied to the received STx-1b batch. The detailed protocol is reported in Annex A.

The obtained high purity Na-form STx-1b montmorillonite was used in the following experiments.

2.1.3 Boom Clay

The Boom Clay sample used in the sorption experiment originates from the non-oxidized BC core with the reference CG72-73W_core 13_section 13.1 sampled within the Putte Member region (12.40-13.35 m intrados) and provided to SCK CEN during the PhD of Yulia Buchatskaya.

2.2 Solid and solution analyses

The purified and dried or freeze-dried IdP and STx-1b and the Boom Clay samples were characterized when relevant for their composition and reactivity. The composition of the samples was characterized by analysing the mineralogy, the Total Organic Carbon and Inorganic Carbon (TOC/TIC) content and the composition of the solutions in equilibrium with the clays. The reactivity of the clays was evaluated by the determination of their surface area and the capacity of the reactive sites.

2.2.1 Semi-Quantitative and Quantitative X-Ray Diffraction

The clay samples, IdP and STx-1b, were analysed in order to detect and, if possible, quantify non-clay mineral impurities.
The clay samples were crushed to a size <150 µm, after which 2.7 g was mixed with 0.3 g of the internal standard zincite (ZnO). Powders were loaded into sample holders with a side-loading technique to minimize preferred orientation of the crystallites. The samples were measured with a Bruker D8 Advance diffractometer, which uses a CuKa1 radiation source, which is filtered with a secondary Ni-ß filter. The diffractometer is equipped with primary and secondary soller slits (2.5°), an automated divergence slit (10 mm irradiated length) and a beam knife located at 1 mm above the sample. The data semi-quantification was done using the Rietveld refinement method.
The bulk BC core from which the BC sample used here is extracted, was analysed at KULeuven (Belgium) during the PhD of Yulia Butchatskaya. Two different subsamples of the core were sampled and analysed. The analysis method included the use of ZnO internal standard and the data quantification was done using the full pattern summation method.

2.2.2 Total Organic and Total inorganic carbon analyses (TOC/TIC)

The TIC/TOC content in solution was measured on an TOC-L (Shimadzu) analyser. The TC (Total Carbon) content is measured with a non-dispersive infrared (NDIR) gas analyser after combustion at 900°C. The TOC content is measured after removing the carbonates by treating the sample with HCl. TIC is calculated by deducting the TOC content from the TC content. Each measurement was repeated at least 3 times and the presented results are the average of the repeated measurements. The uncertainties are calculated based on a validation study performed internally on a series of samples and include the systematic bias, its uncertainty and the reproducibility standard deviation (Thomas, 2018).
The TIC/TOC of the solid samples was measured at the RTW university (Aachen, Germany) on two subsamples of the BC core from which the BC sample used here is extracted.

2.2.3 N_2-adsorption

The specific surface area and pore distribution of the samples were measured with a Micromeritics Tristar II 3020 Surface Area Analyser.
Before starting the measurements, the apparatus was thoroughly flushed with 2 cycles of gas filling and vacuum pulling. The samples were grinded and transferred into empty sample tubes. The sample tubes were then degassed at room temperature during 30 minutes and at 110°C during 24 hours. They were then packed in an isothermal jacket and a dewar flask was filled with liquid N_2. The system was flushed for 5 cycles more and the measurements were started.
The apparatus measures the amount of gas adsorbed by a sample as a function of the relative pressure. By using the theory of Brunauer, Emmett and Teller (BET-theory), the specific surface of the sample can be calculated. The pore diameter and pore volume can be calculated by using the Barrett, Joyner and Halenda method. The BJH theory only applies for mesopores (pore diameter between 2 and 50 nm) and small macropores (pore diameter > 50 nm) and larger and smaller are not resolved by this approach.

2.2.4 ICP-MS and IC

The anionic and cationic composition of the solutions in equilibrium with the purified IdP, STx-1b and BC at a solid/liquid ratio of ~20 g/L (in $NaClO_4$ 0.017 mol/L for IdP and STx-1b and in SPRING for BC) was determined by ICP-MS (after acidification to 2 % HNO_3) and ionic chromatography (IC) analyses. The ICP-MS analyses were performed by the Division of Soil and Water Management of KU Leuven and the IC analyses by the Department of Earth and Environmental Science, Section Geology of KU Leuven.

2.2.5 Potentiometric titrations

The capacity of the sorption sites present on the purified IdP and STx-1b was assessed by mean of potentiometric titrations following the method described by Baeyens and Bradbury (1997) and Bradbury and Baeyens (2009). The experimental protocol is reported in the technical note T-0717 (Thomas and Durce, 2022a).

2.3 Background solutions and experimental conditions

All the used chemicals are ACS or reagent grade.

The objective of this work was to quantify the retention of Sn onto pure clay minerals, i.e IdP and STx-1b montmorillonite and to get a fundamental understanding of the Sn sorption and of its sensitivity to various factors relevant for waste disposal. The determination of the relevant constants needed to describe the Sn sorption (complexation, surface complexation, ionic exchange…) would allow an implementation of the CA approach in a scenario of deep geological disposal in a clay-rich environment such as Boom Clay. To that end, it was chosen to investigate the sorption of Sn(IV) in the conditions detailed in the next paragraph. It should be brought to the reader's attention that experiments performed in $NaClO_4$ were performed at a ionic strength of 0.017 M despite it was originally intended to perform them at 0.015 M. The latter is indeed the ionic strength found at present day in Boom Clay at the Mol site. Unfortunately, a confusion between the monohydrated and anhydrous $NaClO_4$ resulted in an ionic strength of 0.017 M. The small difference of ionic strength is however not expected to impact the sorption of Sn and we assume that the comparison of data obtained in $NaClO_4$ with present day BC conditions is still valid.

2.3.1 Experimental conditions

The sorption of Sn onto IdP and STx-1b was investigated in the following conditions:

- **$NaClO_4$ 0.017 M, pH variable**: Perchlorate is assumed to be non-complexing and the use of sodium perchlorate allows to focus on the pure sorption mechanisms avoiding ligand and competition effect. An ionic strength of 0.015 M was chosen as it is representative of the Boom Clay ionic strength (present day condition at the Mol site). However as previously mentioned the experiments were performed at the slightly higher ionic strength of 0.017 M. Both sorption edges and isotherms were acquired in $NaClO_4$. For sorption edges the pH was varied from 3 to 12. For sorption isotherms, the pH was fixed at ~ 8.4 as it is representative of the present day BC condition at the Mol site.
- **$NaHCO_3$ 0.015 M, pH ~8.4**: The concentration of carbonate varies with the considered clay-rich environment and its potential influence on sorption will vary accordingly. The use of $NaHCO_3$ 0.015 M was chosen to evaluate the impact of carbonate in comparison to the carbonate free system $NaClO_4$ 0.017 M and to be representative of the present day BC conditions at the Mol site. As for the other systems, the pH was fixed at ~8.4 to be representative of present day BC conditions at the Mol site.
- **Synthetic Seawater (SSW), pH ~8.4**: Depending on the localization and depth of the considered clay-rich formation, the salinity of the pore solution could vary significantly. The use of SSW was taken as an extreme of this variation to evaluate the influence of salinity on the sorption in comparison to the low saline system $NaClO_4$ 0.017 M and in agreement with the works of (Durce et al., 2020b; Van Laer, 2018; Van Laer et al., 2020). The pH of SSW in equilibrium with BC is expected around 7.4 (Salah and Wang, 2018) but it was here chosen to work at a pH of ~8.4 to focus on the sole role of salinity in Sn sorption and avoid any additive pH effect.
- **$NaClO_4$ 0.017 M, BC Dissolved Organic Matter (5 or 12 ppmC), pH ~8.4**: As for the salinity, the concentration of dissolved organic matter (DOM) in the pore solution varies depending on the considered host formation and location. In the case of BC at the Mol site, for instance, the concentration of DOM measured in solution is in average 108-115 mgC/L (De Craen et al., 2004; Durce et al., 2015) while in other locations like in Essen it is lower. The presence of DOM was evidenced in a previous work to control the speciation of Sn(IV) (Durce et al., 2020a; Durce et al., 2020b) and it is important to assess its effect on sorption. According to Sn(IV)-DOM complexation constants determined by Durce et al. (2020b), Sn(IV) would mainly exist as complexed to DOM from already low DOM concentrations. This is the reason why DOM concentration in the present work was limited to 5-12 ppmC. As for the other systems, the pH was fixed at ~8.4 to be representative of present day BC conditions at the Mol site.

To verify the applicability of the determined constants on the pure clay minerals and of the CA approach to the sorption of Sn(IV) onto Boom Clay in present day conditions, a sorption isotherm onto BC was also acquired in **SPRING water at pH ~8.4**.
Details on the used background solutions and their preparation are provided in the following paragraphs.

2.3.2 $NaClO_4$, $NaHCO_3$ and SSW

$NaClO_4$ and $NaHCO_3$ solutions were prepared from the corresponding salts i.e $NaClO_4$ anhydrous and $NaHCO_3$,H_2O dissolved in degassed ultrapure water directly in an N_2-atmosphere glovebox. Mother solutions of higher concentration, i.e 0.023 M for $NaClO_4$ and 0.02 M for $NaHCO_3$, were made to be further diluted when preparing the clay suspensions and samples for the sorption experiments. To avoid the perturbation of the clay materials, KCl salt was also added to the mother solution to a concentration of 1.3×10^{-4} mol/L.

The synthetic seawater (SSW) was prepared based on the composition reported by Kester et al. (1967) and detailed in Table 1. It was prepared in an N_2-atmosphere glovebox with the use of degassed ultrapure water according to the detailed procedure reported in Appendix B.

Table 1. Composition of the synthetic seawater (SSW) (based on Kester et al. (1967))

Species		Concentration (g/L)	Concentration (mM)
Cations	Na^+	10.80	468
	K^+	0.387	9.90
	Ca^{2+}	0.414	10.3
	Mg^{2+}	1.295	53.3
	Sr^{2+}	0.008	0.09
Anions	Cl^-	19.4	547
	SO_4^{2-}	2.71	28.2
	HCO_3^-	0.142	2.33
	Br^-	0.066	0.82

The pH of the prepared solutions was not checked and was adjusted later on when preparing the samples for the sorption experiments. The concentration of Sn and other cationic impurities in the solutions was measured by ICP-MS by the Division of Soil and Water Management of KU Leuven and is reported in Appendix C.

2.3.3 SPRING pore water

The SPRING pore water was collected from the horizontally-oriented piezometer TD-116E, installed at the level of the HADES laboratory (-196.6 m TAW (Tweede Algemene Waterpassing)). The piezometer is entirely made of stainless steel and contains 4 filters of 1.5 m length directly in contact with Boom Clay and with a pore size distribution from 7 to 16 µm. Pore water was collected from the four interconnected filters from 2021-03-31 to the 2021-05-19. The water collected during this period was given the reference TD-116E-all/2021-05-19, but for the sake of simplicity, in this report it will be referred to as SPRING water. The concentration of Sn and other cationic impurities in the solutions was measured by ICP-MS by the Division of Soil and Water Management of KU Leuven and is reported in Appendix C. The content of organic and inorganic carbon (TOC and TIC) was measured as described in section 2.2.2. The measured values were 133 ± 27 mgC/L and 82 ± 25 mgC/L for TIC and TOC, respectively.
Prior to the sorption experiments, the SPRING water was filtered at 0.45 µm (PVDF hydrophilic, VWR).

2.3.4 DOM isolation and characterization

The DOM used in the sorption experiments was extracted from the pore water collected from the EG/BS piezometer (S-1D) following the same procedure as described previously (Durce et al., 2020a; Durce et al., 2020b), but in a N_2-glovebox. Only the main steps will be repeated here.

In a N_2-glovebox, the EG/BS water was first filtered at 0.45 µm (PVDF, VWR) and then ultrafiltered at 1 kDa on regenerated cleaned cellulose membranes (Ultracel 76 mm 1 kDa NMWL, Millipore). The residual solution on the UF membrane was recovered in a small volume of $NaClO_4$ 0.017 M and further purified by dialysis at 1 kDa against $NaClO_4$ 0.017 M (Regenerated cellulose membrane Spectra/Por7, 18*11.5 mm). The dialyzed solution was then stored in a dark bottle in the glovebox until further use and referred to as DOM_$NaClO_4$.

The concentration of dissolved organic carbon in DOM_$NaClO_4$ was determined by TOC/TIC measurements as described in section 2.2.2. The UV-Vis absorbance at 280 and 254 nm was also measured. The size distribution was measured by size exclusion chromatography as described in Durce et al. (2015). The concentration of natural Sn in DOM_$NaClO_4$ was not quantified, but DOM being isolated from EG/BS pore water and according to the same procedure as reported in Durce et al. (2020b), it is assumed to have similar properties as the batches isolated in our previous work. The Sn content is therefore assumed to be of the same magnitude as measured by Durce et al. (2020b), i.e $< 1 \times 10^{-6}$ mol/gC. The same reasoning is valid for the nature and concentration of cationic impurities and the proton exchange capacity which are assumed equal to the values reported for the batch Batch2_NaHCO3_02, *i.e* PEC_{eff}=10.7 ± 2.1 meq/gC (Durce et al., 2020b).

The measured properties of DOM_$NaClO_4$ are summarized in Table 2 and Figure 1.

Table 2. TIC/TOC and UV absorbance of DOM_$NaClO_4$ solution

TOC (mgC/L)	877 ± 263
TIC (mgC/L)	8 ± 1
UV_{280}/UV_{254} (cm^{-1})	32.11/39.17

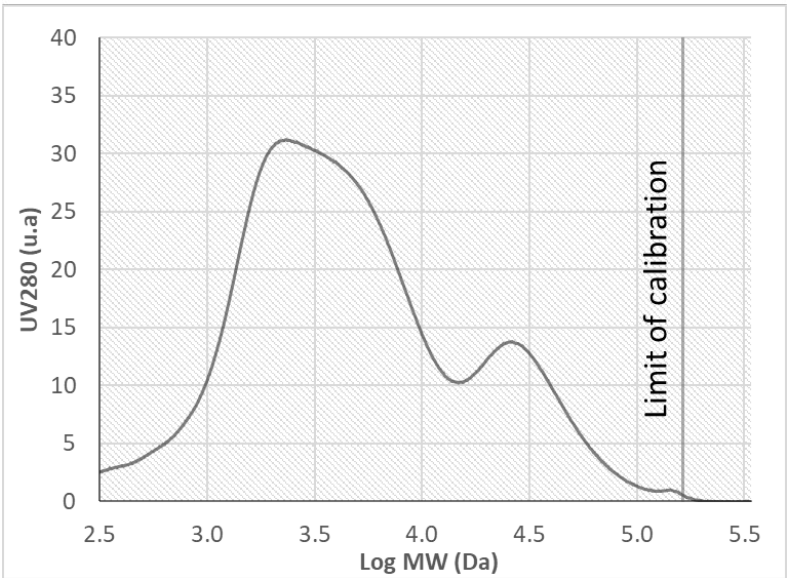

Figure 1. Molecular Weight Distribution of DOM_$NaClO_4$ measured by SEC/UV280

2.4 ^{113}Sn solution and gamma counting

To allow working at low concentration, it was chosen to work with the radioactive isotope ^{113}Sn with a half-life of 115.09 days. A source of $SnCl_4$ in 6 M HCl was purchased from Eckert and Ziegler with a total activity of 0.1 mCi, a specific activity of 7.5 × 10^5 Bq/mL (at the date of purchase) and a carrier concentration of 4.21 × 10^{-4} mol/L. Two ^{113}Sn solutions were purchased and used over the study duration. The total concentration of Sn in the ^{113}Sn solution purchased in September 2020 was not cross-checked by ICP-MS and is assumed to match the value given by the supplier. The second solution, purchased in January 2021, displayed a Sn concentration of 3.01 × 10^{-4} mol/L when measured by ICP-MS.

Various sub-solutions of the original spike were prepared by dilution in ultrapure water or HCl and used in the experiments. For practical reasons, the solutions were prepared outside the glovebox, but were always allowed to equilibrate afterwards with the atmosphere of the glovebox (N_2).

^{113}Sn is a quasi-monoenergetic gamma emitter in the energy region around 390 keV and is analysed in this work by gamma-counting on a Packard Cobra Quantum counter on the energy range 300-500 keV. The counting efficiency, ε, on this range was investigated in a previous study in UP water, $NaHCO_3$ 0.015 M and synthetic seawater and was evaluated based on the activity supplied by the provider to 0.35 ± 0.02 (Durce et al., 2020a). From January 2021, the efficiency was observed to have dropped to 0.29, probably due to a lower specific activity of the second purchased ^{113}Sn source. The counting efficiency of the clay-containing suspensions was observed to be identical to the solution, at least until a S/L ratio of 1 g/L. The total concentration of Sn in the samples is calculated from the measured activity as:

$$[Sn] = \frac{(CPM_s - CPM_b)}{V_s \times 60 \times 0.35\ (or\ 0.29) \times e^{\left(-\frac{ln2}{t_{1/2}} \times \Delta t\right)}} \times \frac{C_0}{A_0} \quad (1)$$

With CPM_s and CPM_b, the measured counts (CPM) of the sample and the blank, respectively, V_s (mL), the measured volume of sample, $t_{1/2}$ (days), the half-life of ^{113}Sn, Δt (days), the time span between the day of measurement and the reference date on the activity certificate, C_0 (mol/L), the Sn concentration of the source and A_0 (Bq/mL), the initial activity of the ^{113}Sn source.

The uncertainty associated to the Sn concentration is calculated by propagating the experimental errors (confidence limit of 95 %) with $2\sigma(\frac{C_0}{A_0})/\frac{C_0}{A_0} = 0.1$, corresponding to the measurement error on C_0, $2\sigma(V_s)/V_s$ which was neglected and assumed null, $2\sigma(\varepsilon)/\varepsilon = 0.06$ corresponding to the average of the experimental error on the efficiency, ε.

2.5 Sorption Experiments

All the experiments were performed in a glovebox under inert atmosphere (Ar). A maximum background of 2 ppm O_2 is assumed.

2.5.1 Clay suspensions

Due to the expected high sorption of Sn(IV) onto clay minerals, the sorption experiments were performed at low solid/liquid ratios. Directly preparing these low ratios is practically difficult due to the low amount of solid to weigh. 'Mother suspensions' were then prepared with a S/L of ~20 g/L and diluted further to achieve the desired solid/liquid ratios in the sorption experiments.
The mother suspensions were prepared in the glovebox from the clay materials described in section 2.1. The purified IdP was suspended into 0.017 M $NaClO_4$ + 1 × 10^{-4} mol/L KCl. Two different suspensions were prepared and used over the course of the study. They are referred to as IdP_0 and IdP_1. For STx-1b, one suspension was prepared from the suspension obtained at the end of the purification procedure (before freeze-drying) and one from the freeze-dried solid. In the first case, the suspension at 147 g/L of purified STx-1b in 0.01 M $NaClO_4$ was vigorously stirred, a sample taken and diluted into $NaClO_4$ 0.023 M/Ultrapure water to reach a final composition of 0.017 M $NaClO_4$+ 1 × 10^{-4} mol/L KCl. It is referred to as STx1b_0. The freeze-dried STx-1b was directly suspended into 0.017 M $NaClO_4$+ 1 × 10^{-4} mol/L KCl. It is referred to as STx1b_1. The Boom Clay core was peeled and directly dispersed into the filtered SPRING water. The suspension is referred to as BC_1.
The suspensions were stirred for at least 1 day. They were then allowed to settle down, in some cases, the pH was measured and the supernatants were analysed by ICP-MS and IC as described in section 2.2.4.
The solid/liquid ratio of the suspensions was determined by measuring the weight loss at 105 °C and the results are summarized in Table 3. The solid/liquid ratio of the STx1b_0 suspension was measured twice over the course of the study to account for possible evaporation with time. The two measurements are referred to STx1b_0a and STx1b_0b.

Table 3. Measured solid/liquid ratio and pH of the mother clay suspensions. n.m= not measured

	Solid/liquid (g/L)	Solution	pH
IdP_0	26	$NaClO_4$ 0.011 M (+KCl 1 ×10^{-4} M)	7.16
IdP_1	21	$NaClO_4$ 0.017 M (+KCl 1 ×10^{-4} M)	n.m
STx1b_0a	22	$NaClO_4$ 0.017 M (+KCl 1 ×10^{-4} M)	7.51
STx1b_0b	24	$NaClO_4$ 0.017 M (+KCl 1 ×10^{-4} M)	n.m
STx1b_1	20	$NaClO_4$ 0.017 M (+KCl 1 ×10^{-4} M)	n.m
BC_1	13	SPRING	10.14

2.5.2 Sorption Edges onto IdP and STx-1b

To evaluate the effect of pH on the sorption of Sn(IV) on pure clay minerals, sorption edges were acquired on the purified IdP and STx-1b from pH 3 to pH 12. The role of cation exchange mechanism in the sorption of Sn(IV) can be assumed negligible, Sn(IV) hydrolysing from already low pH. It was, in consequence, chosen to work at a fixed ionic strength as to know 0.017 M to be representative of or close to the present day Boom Clay conditions at the Mol site. The sorption edges being acquired in $NaClO_4$ to avoid any ligand and competition effect (see section 2.3), a direct comparison with the published data of Bradbury and Baeyens (2005b) and Bradbury and Baeyens (2009) obtained at a ionic strength of 0.1 M should be possible and allow to confirm or infirm the negligible role of cation exchange in Sn(IV) sorption onto clay minerals.

The sorption of Sn(IV) on each clay was measured over 18 pH points ranging from pH 3 to pH 12 at a Sn concentration of (6.8 ± 0.4) ×10^{-8} mol/L and (6.7 ± 1.2) ×10^{-8} mol/L for IdP and STx-1b, respectively. The experiments were performed into 50 mL PPCO centrifugal tubes (Nalgene, VWR) with a solution volume of 20 mL and a solid/liquid ratio of 0.65 ± 0.02 and 0.54± 0.02 g/L for IdP and STx-1b, respectively. The pH was maintained with the use of pH buffers as reported in Table 4. The concentration of the buffers in the experiments was fixed at 2×10^{-3} mol/L and stock solutions of 0.2 mol/L were prepared

in ultrapure water. All the glass- and plasticware were acid-washed before use. The samples were prepared according to the following procedure: In an N_2-glovebox, the right volumes of 0.017 M $NaClO_4$ solution, pH buffer, base or acid (NaOH 0.5 M or $HClO_4$ 0.5M) and ^{113}Sn solution were added to the tubes. The concentrations of the base and acid forms of the pH buffers and the volume of acid/base to be added to fix the pH are calculated according to Equations (2) to (5).

$$[HA] = \frac{C_{tot}}{1 + 10^{pH-pKa}} \quad (2)$$

With [HA], the concentration of the buffer in acid form (mol/L), C_{tot}, the total concentration of the buffer (mol/L), pH the target pH and pKa, the acid dissociation constant of the buffer

$$[A^-] = [HA] \times 10^{pH-pKa} \quad (3)$$

With $[A^-]$, the concentration of the buffer in base form (mol/L).

$$V_{base} = [A^-] \times \frac{V_{tot}}{C_{base}} \quad (4)$$

With V_{base}, the volume (mL) of base solution to be added with a buffer in acid form, V_{tot} (mL), the total volume of the sample and C_{base} (mol/L), the concentration of the base solution.

$$V_{acid} = [HA] \times \frac{V_{tot}}{C_{acid}} \quad (5)$$

With V_{acid}, the volume (mL) of acid solution to be added with a buffer in base form, V_{tot} (mL), the total volume of the sample and C_{acid} (mol/L), the concentration of the acid solution.

It should be noted that base was also added to neutralize the acidity brought by the addition of Sn (in acid solution) to the sample.
For pH < 4.5 and > 10, no pH buffer was added to the samples and the pH was adjusted to the target value with the addition of NaOH or $HClO_4$ 0.5 M.

Table 4. List of used pH buffers

	pKa	pH range	type
Acetic acid	4.76	4.3-5.3	solution 99.8 %
MES	6.15	5.7-6.7	acid, solid
MOPS	7.2	6.8-7.7	sodium salt
TRIS	8.06	7.5-8.5	HCl acid, solid
CHES	9.55	9-10	acid, solid

The tubes were shaken on a mechanical shaker for 1 h and the pH was controlled and adjusted if needed with $HClO_4$ or NaOH 0.5 M. Then, 0.5 mL of the vigorously stirred clay suspension IdP_0 or STx1b_0 was added and the tubes were shaken again for 1 h. The pH was controlled once more and adjusted if needed with the $HClO_4$ or NaOH 0.5 M solutions. The tubes were put under agitation on a mechanical shaker for 7 days. 1 mL of the suspensions was then sampled and analysed by gamma counting. Attention was paid to homogenize the suspensions by vigorously shaking them right before sampling. The tubes were taken out of the glovebox, centrifuged for 1 h at 20 000 × g and gently reintroduced in the glovebox. The centrifugation step should allow to settle particles down to 20 nm (Equation (6)).

$$d^2 = \frac{18\eta}{(\rho - \rho_w)4\pi^2\varpi^2 t} ln\frac{r_{max}}{r_{min}} \quad (6)$$

With η (kg/(m.min)), the dynamic viscosity, ρ and ρ_w (g/cm^3), the particle and solvent density, respectively, ϖ (RPM), the centrifugation speed in revolution per minute, t (min), the centrifugation time, r_{min} and r_{max} (m) the shortest and longest radial position, respectively and d (m), the diameter of the particle (m).
1 mL of the supernatants was sampled and analysed by gamma counting and the pH of the supernatants was measured. To check the sorption of Sn on the tubes and the possible Sn loss during centrifugation, 3 blanks were prepared in parallel with respective pH of 3, 7 and 12. The blanks were prepared following the same procedure as the samples, but without addition

of the clay suspension. More information on the weighed volumes used in each sample and blank can be found in the electronic files embedded at the end of the report.

2.5.3 Sorption Isotherms onto IdP and STx-1b and Boom Clay

Clay minerals are assumed to bear different types of amphoteric surface hydroxyl groups with different acidity and displaying different sorption affinity and capacity. The so-called strong sites have generally a low capacity, but a high affinity constant, while weak sites are more abundant, but display a lower affinity constant. The 2-site protolysis-non electrostatic surface model (2SPNE) was developed to describe the protonation/deprotonation of these sites and combined to surface complexation and cation exchange (SC/CE) it is largely used to describe sorption onto illite and montmorillonite.
The existence of different sorption sites would lead to a non-linear sorption when working over a large solute concentration range. To evaluate the sorption linearity of Sn(IV) on pure clay minerals, sorption isotherms were acquired on the purified IdP and STx-1b in the conditions described in section 2.3 . All the isotherms were acquired at a pH ~8.4 and the experimental protocols followed for the different conditions are described in the following paragraphs. The ranges of concentration to be investigated were fixed on two constraints: the detection limit of the liquid scintillation counting and the solubility limit of Sn in the experimental conditions. Based on the calculation performed by Salah and Wang (2017, 2018) and reported by Durce et al. (2020b) the Sn solubility under present day BC conditions and in SSW would be 1.89×10^{-7} mol/L and 7.0×10^{-8} mol/L, respectively. In presence of clay minerals, the fast sorption of Sn is expected to limit precipitation allowing to extend the working range of Sn concentration. To cover a good range of concentration while remaining within the same order of magnitude as the solubility limit, the upper concentration limit at which the sorption experiments could be performed was fixed at 6.0×10^{-7} mol/L. On the other side, considering the high Sn(IV) sorption on clays and the detection limit of the liquid scintillation counting, the lower concentration limit was fixed at 1×10^{-9} mol/L. Two different solid/liquid ratios had to be used to cover the chosen range of concentrations.
An additional sorption isotherm was acquired on Boom Clay to assess the sorption of Sn(IV) and evaluate, as previously mentioned, the applicability of the CA approach. The followed experimental protocol is also described in this section.

The protocol followed for the different conditions and the different clays, i.e IdP, STx-1b and BC was sensibly the same. The sorption of Sn(IV) was measured for the different conditions over 7 concentration points on IdP and 8 concentration points on STx-1b and BC. For each concentration, three replicates were prepared. The ranges of Sn concentrations used for each experiment are summarized in Table 5. The experiments were all performed into 50 mL PPCO centrifugal tubes (Nalgene, VWR) with a solution volume of 20 mL. To allow measurable ^{113}Sn activity over the studied range of concentrations two solid/liquid ratios were used in the experiments performed on IdP and STx-1b. The values of the used solid/liquid ratio are reported in Table 5. The pH of the experiments was initially fixed to 8.4 and maintained with the use of TRIS buffer at a concentration of 2×10^{-3} mol/L. All the glass- and plasticware were acid-washed before use.
The samples were prepared according to the following procedure: In an N_2-glovebox, 200 µL of TRIS buffer stock solution at 0.2 mol/L, the right volumes of $NaClO_4$/ $NaHCO_3$/SSW/SPRING solution, NaOH 0.5 M (to adjust the pH to 8.4, see section 2.5.2) , ^{113}Sn solution and when relevant of DOM_NaClO4 were added to the tubes. The tubes were shaken on a mechanical shaker for 1 h and the pH was controlled and adjusted to 8.4 if needed with $HClO_4$ or NaOH 0.5 M. Then, 0.1 or 0.5 mL of the vigorously stirred clay suspension IdP_1, STx1b_0(a or b) or BC_1 was added and the tubes were shaken again for 1 h. The pH was controlled once more and adjusted if needed with the $HClO_4$ or NaOH 0.5 M solutions. The tubes were put under agitation on a mechanical shaker for 7 days. In the case of IdP, extra sorption points were performed in NaClO4 0.017 M later on in the study. The contact time for these points was reduced to 4 days, which was judged to be sufficient to reach the sorption equilibrium.1 mL of the suspensions was then sampled and analysed by gamma counting. Attention was paid to homogenize the suspensions by vigorously shaking them right before sampling. The tubes were taken out of the glovebox, centrifuged for 1 h at 21 000 × g for IdP and STx-1b and 2 h at 21 000 × g for BC and gently reintroduced in the glovebox. 4 mL of the supernatants were sampled and analysed by gamma counting and the pH of the supernatants was measured. The average equilibrium pH values are reported in Table 5. To check the sorption of Sn on the tubes and possible Sn loss during centrifugation, three blanks were prepared in parallel of each experimental set with respective Sn(IV) concentration as indicated in Table 5. The blanks were prepared following the same procedure as the samples, but without addition of the clay suspension. In addition, in the case of BC, two blank BC suspensions were also run in parallel to estimate the concentration in solution of natural Sn. The blank suspensions were prepared following the same procedure as the samples, but without addition of ^{113}Sn. At the end of the contact time, the blank BC suspensions were centrifuged for 2 h at 20,000× g and the supernatant analysed for Sn concentration by ICP-MS.
More information on the weighed volumes used in each sample and blank can be found in the electronic files embedded at the end of the report.

Table 5. Experimental conditions for sorption isotherms on IdP, STx-1b and BC. (1) pseudo-equilibrium at 7 days, (2) error of TOC measurements. SD= standard deviation.

Clay material	Solution	Sn(IV) concentration range (mol/L)	Solid/liquid ratios (g/L) (± SD)	Average DOM concentration (mgC/L) (± error of measurement)	Average pH measured at equilibrium(1) (± SD)	Sn(IV) concentration (mol/L) in blanks (± SD)
IdP	$NaClO_4$ 0.017 M	3.3×10^{-9} to 4.2×10^{-7}	0.10 ± 0.002 ,0.51± 0.02 and 0.53 ± 0.02	/	8.56 ± 0.10 and 8.49 ± 0.04	(2.90 ± 0.02) $\times10^{-8}$
STx-1b	$NaClO_4$ 0.017 M	1.1×10^{-9} to 4.2×10^{-7}	0.10 ± 0.004 and 0.50 ± 0.1	/	8.31 ± 0.06	(2.05 ± 0.02) $\times10^{-8}$
IdP	$NaClO_4$ 0.017 M	1.9×10^{-9} to 3.0×10^{-7}	0.10 ± 0.02 and 0.46± 0.04	4.5 ± 2.8	8.37 ± 0.06	(2.87 ± 0.02) $\times10^{-8}$
STx-1b	$NaClO_4$ 0.017 M	5.5×10^{-9} to 1.2×10^{-7}	0.11 ± 0.004 and 0.56± 0.14	11.9 ± 7.2	8.43 ± 0.14	(4.7± 7.2) $\times10^{-8}$
IdP	$NaHCO_3$ 0.015 M	1.7×10^{-9} to 3.0×10^{-7}	0.09 ± 0.02 and 0.52± 0.02	/	8.66 ± 0.32	(2.89 ± 0.10) $\times10^{-8}$
STx-1b	$NaHCO_3$ 0.015 M	2.1×10^{-9} to 4.3×10^{-7}	0.10 ± 0.002 and 0.49 ± 0.008	/	8.51 ± 0.04	(2.05 ± 0.02) $\times10^{-8}$
IdP	SSW	1.8×10^{-9} to 4.0×10^{-7}	0.10 ± 0.002 and 0.51± 0.004	/	8.36 ± 0.06	(2.84 ± 0.14) $\times10^{-8}$
STx-1b	SSW	1.5×10^{-10} to 3.9×10^{-7}	0.10 ± 0.006 and 0.52± 0.04	/	8.24 ± 0.08	(1.9 ± 0.4) $\times10^{-8}$
BC	SPRING	9.9×10^{-10} to 5.6×10^{-7}	0.13 ± 0.01	82 ± 25	8.41 ± 0.04	(2.5 ± 0.2) $\times10^{-8}$

2.5.4 Effect of the solid/liquid ratio on Sn(IV) sorption on STx-1b in $NaClO_4$ 0.017 M

The sorption isotherms obtained in STx-1b and further presented in 3.2.2 showed an effect of the solid/liquid ratio on the sorption of Sn(IV) in most of the investigated conditions. To investigate this effect in more details, the sorption of Sn(IV) on STx-1b was investigated on two series of experiments performed with various solid/liquid ratios in $NaClO_4$ 0.017 M. The sorption of Sn(IV) was measured over five solid/liquid ratios for each series at a fixed Sn(IV) concentration. In the first series, two replicates were prepared per solid/liquid ratio, while in the second series only unique points were acquired, this second series being intended as a repeat of the first one. The experimental conditions of the experiments are summarized in Table 6. As for the sorption edges and the sorption isotherms acquired in this work, this experimental set was also performed into 50 mL PPCO centrifugal tubes (Nalgene, VWR) with a solution volume of 20 mL and at an initial pH fixed to ~8.4 and maintained with the use of TRIS buffer at a concentration of 2×10^{-3} mol/L. All the glass- and plasticware were acid-washed before use.

The samples of each series were prepared according to the following procedure: In an N_2-glovebox, 200 µL of TRIS buffer stock solution at 0.2 mol/L, the right volumes of $NaClO_4$ solution, NaOH 0.5 M (to adjust the pH to 8.4, see section 2.5.2) , ^{113}Sn solution were added to the tubes. The tubes were shaken on a mechanical shaker for 1 h and the pHs were controlled and adjusted to 8.4 if needed with $HClO_4$ or NaOH 0.5 M. The right amount (depending on the target S/L) of the vigorously stirred clay suspension STx-1b_1 was added and the tubes were shaken again for 1 h. The pH was controlled once more and adjusted if needed with the $HClO_4$ or NaOH 0.5 M solutions. The tubes were put under agitation on a mechanical shaker for 7 days. 1 mL of the suspensions was then sampled and analysed by gamma counting. Attention was paid to homogenize the suspensions by vigorously shaking them right before sampling. The tubes were taken out of the glovebox, centrifuged for 2 h at 21 000 × g and gently reintroduced in the glovebox. 4 mL of the supernatants were sampled and analysed by gamma counting and the pH of the supernatants was measured. The average equilibrium pH values are reported in Table 6. To check the sorption of Sn on the tubes and possible Sn loss during centrifugation, two blanks were prepared in parallel of each experimental series with respective Sn(IV) concentration as indicated in Table 6. The blanks were prepared following the same procedure as the samples, but without addition of the clay suspension. In addition, in the first experimental set, four blank suspensions were also prepared to assess the evolution of the composition of the solution with the solid/liquid ratio at equilibrium. These blanks were prepared at different solid/liquid ratios as reported in Table 6. They were prepared and sampled according to the same procedure as the samples, but without addition of ^{113}Sn solution. The supernatants were then acidified and sent for ICP-MS analyses to the Division of Soil and Water Management of KU Leuven.

More information on the weighed volumes used in each sample and blank can be found in the electronic files embedded at the end of the report.

Table 6. Experimental conditions for sorption at different solid/liquid ratios on STx-1b SD= standard deviation.

Experimental series	Sn(IV) concentration (mol/L) (± SD)	Solid/liquid ratios (g/L)	Average pH measured at equilibrium(1) (± SD)	Sn(IV) concentration (mol/L) in blanks (± range)	Solid/liquid ratios blank suspensions (g/L)
1	(5.71 ± 0.12) ×10^{-8}	0.09 to 1.22	8.20 ± 0.04	(5.73 ± 0.06) ×10^{-8}	0.10 to 1.24
2	(6.03 ± 0.14) ×10^{-8}	0.10 to 1.20	8.39 ± 0.06	(6.10 ± 0.02) ×10^{-8}	/

2.5.5 Calculation of the solid-liquid distribution coefficients (K_d)

The extent of sorption of Sn(IV) on the different substrates and background solutions is represented by the solid-liquid distribution coefficients referred to as R_d (L/kg), and calculated according to Equation (7).

$$R_d = \frac{Sn_0 - Sn_{eq}}{Sn_{eq}} \times \frac{V}{m} \quad (7)$$

With Sn_0 (mol/L), the concentration in the suspension before centrifugation, Sn_{eq} (mol/L), the concentration in the supernatant after centrifugation, V(L), the volume of solution and m (kg), the mass of clay. Both concentrations are calculated based on the measured activities using Equation (1).

The calculated R_d values are provided with their associated uncertainties calculated with the propagation of errors as reported in Appendix F.

2.6 Modelling

2.6.1 General approach

The thermodynamic sorption model(s) used here to describe the obtained experimental data were all implemented in the PHREEQC Version 3 geochemical code from the US Geological Survey (Parkhurst and Appelo, 2013) and the calculations were done with the Thermochimie V10a database (Grivé et al., 2015) using the extended Debye-Hückel equation (B-dot). Only the activity coefficients of DOM and $SnDOM^{+3}$ were calculated based on the Davies equation, as the ion size parameter for these species is unknown. All the modelling was performed for a temperature of 25 °C.

The experimental data obtained on IdP are modelled using the 2SPNE SC/CE model developed by Bradbury and Baeyens (1997) to describe the sorption of cations on Montmorillonite SWy and further extended to Illite du Puy (Bradbury and Baeyens, 2009). As discussed by Bradbury and Baeyens (2005b), Sn(IV) is expected to hydrolyse from low pH and the contribution of cation exchange in its sorption can be assumed negligible. The model applied to the present data can therefore be reduced to a 2SPNE SC model in which the contribution of the cation exchange for Sn(IV) is neglected. The selectivity coefficients for the major cations are taken equal to the values reported by Bradbury and Baeyens (2009) and summarised in Appendix D.
Within the 2SPNE SC model, the protolysis behaviour of the clay minerals is described by two different weak sites ($\equiv S^{W1}OH$ and $\equiv S^{W2}OH$) of same capacity, but with different protolysis constants. A strong site with high affinity to metal sorption ($\equiv S^{s}OH$) is also present with a low capacity and displaying the same protolysis constants as the $\equiv S^{W1}OH$ sites. In the range of concentrations investigated here, Sn(IV) was assumed to sorb only on the strong-type sites of IdP and, though the weak sites were implemented in the model, they did not contribute to Sn(IV) sorption.
The protolysis constants of IdP and the capacity of the weak sites are fixed on the values determined by Bradbury and Baeyens (2009) and reported in Appendix D. The capacity of the strong sites of IdP determined by Bradbury and Baeyens (2009) is reported in Appendix D. In some of the modelling exercises, this capacity is allowed to vary in order to better describe the experimental data.

Due to the effect of the solid/liquid ratio observed on the sorption of Sn(IV) onto the Montmorillonite STx-1b and the uncertainty on which solid/liquid ratio would provide the most accurate data (see section 3.2.2), it was chosen to not work further on the modelling of the experimental datasets obtained on STx-1b. Should new experimental data shed light on the effect of the solid/liquid ratio, the datasets could later be modelled and the results reported in a further report/publication. Yet, to compare our data to the previously reported data of Bradbury and Baeyens (2005b) and Bradbury and Baeyens (2017), the 2SPNE SC/CE model using the constants reported for Montmorillonite SWy-1 by the same authors (Appendix D and Table 7) was implemented and applied to the sorption edge and sorption isotherm obtained in $NaClO_4$ 0.017 M. To be consistent with the model of Bradbury and Baeyens (2005b) and Bradbury and Baeyens (2017), this modelling exercise was performed by using the same set of Sn(IV) hydrolysis constants than the authors (Table B3) and not the one of the Thermochimie database. The model and its outcome are referred as 'Model0 MoMo'. An extra modelling exercise was also performed with the same Sn(IV) surface complexation constants (Table 7), but using the STx-1b hydrolysis constants and site capacities as determined by Thomas and Durce (2022b) and reported in Table 15. This model is referred to as 'Model1 MoMo'. For none of the models, constant optimization was performed and the models were not extended to the other investigated experimental conditions.

Table 7. Sn(IV) surface complexation reactions and the reported constants on Illite du Puy and Montmorillonite Na-SWy-1 by (1) Bradbury and Baeyens (2009) and (2) Bradbury and Baeyens (2017)

		Ilite du Puy(1)	Montmorillonite Na-SWy-1(2)
$\equiv S^sOH + Sn^{4+} + 2H_2O \leftrightarrow \equiv S^sOSn(OH)_2^{+} + 3H^+$	$log\ K_1$	12.5	13.3
$\equiv S^sOH + Sn^{4+} + 3H_2O \leftrightarrow \equiv S^sOSn(OH)_3 + 4H^+$	$log\ K_2$	8.5	9.15
$\equiv S^sOH + Sn^{4+} + 4H_2O \leftrightarrow \equiv S^sOSn(OH)_4^{-} + 5H^+$	$log\ K_3$	2.5	1.6
$\equiv S^sOH + Sn^{4+} + 5H_2O \leftrightarrow \equiv S^sOSn(OH)_5^{2-} + 6H^+$	$log\ K_4$	-5.7	-7.6

One of the main difficulties with the modelling of Sn(IV) sorption is the lack of available thermodynamic data describing the Sn(IV) speciation. In their work, Bradbury and Baeyens (2009) used data published by Hummel et al. (2002) and data from Baes and Mesmer (1977) that they converted to $log\ K$ using the Davies relation (Davies, 1962). On the other hand, the NEA book (Gamsjäger et al., 2012), which generally serves as reference for thermodynamic constants, selected a different set of hydrolysis constants. In their review, the authors validated only the fifth and sixth hydrolysis constants (Appendix D) with reactions written with $Sn(OH)_4$ as major species. The constants integrated in the Thermochimie V10a database, which we used in our previous work on Sn(IV) (Durce et al., 2020b), are derived from the constants validated by Gamsjäger et al. (2012). Despite that they were recalculated to Sn^{4+}using an extra constant for the fourth hydrolysis, they remain until today, the best set of Sn(IV) hydrolysis constants available and were used here in all the modelling exercises.
In addition to the uncertainty on the Sn(IV) hydrolysis, there exists also a significant lack of thermodynamic data regarding the complexation of Sn(IV) with relevant inorganic ligands such as carbonates. Neither the NEA book (Gamsjäger et al., 2012) nor the Thermochimie V10a database contain any reaction for Sn(IV)-carbonate complexation. This absence of data makes the prediction of the effect of carbonate on the Sn(IV) complexation difficult. With regards to the lack of thermodynamic data, the sorption data obtained here in presence of carbonate, in $NaHCO_3$ 0.015 M, can only be modelled by imposing a Sn(IV)-carbonate reaction and optimizing the corresponding constant to fit the experimental data as described more in detail in section 2.6.2.4. It is evident that the obtained constant is highly conditional to the experimental conditions used here and to the formalism chosen for the complexation reaction.

In this study we assume the large predominance of Sn(IV) over Sn(II) in our experimental conditions. This was confirmed by thermodynamic calculations using both the MOLDATA and Thermochimie V10a database and assuming a background of 2 ppm of O_2 (pO_2=-5.7).

The calculated $log\ R_d$ values were modelled by adjusting the relevant constants and the strong sorption site capacity. The optimization of the constants was done using the UCODE_2014 program from the US Geological Survey (Poeter et al., 2014) with or without the use of singular-value decomposition and by minimizing the weighted least-squares objective function with respect to the constant values using a modified Gauss–Newton method. The uncertainty on the determined constants and the sorption site capacity was estimated from a sensitivity analysis with respect to the input parameters. The approach followed for this analysis is not described here but the details can be found in the Supplementary Materials of Durce et al. (2022). The boundary of the confidence interval for each fitted parameter was taken as the largest negative and positive variations induced by the uncertainty on the selected input parameters.

Various models were tested to be representative of the different experimental conditions and to describe the experimental data. More details on these models and on the reasoning of their development are provided in the following section. A summary of the chemical reactions implemented in the various modelling exercises is given in Table 8. The occurrence of these reactions in the different models tested here and the origin of their constant value are detailed in Table 9, Table 10 and Table 11.

Table 8. Aqueous and surface complexation reactions implemented in the different models used to describe the sorption experimental dataset.

$\equiv S^sOH + Sn^{4+} + 4H_2O \leftrightarrow \equiv S^sOSn(OH)_4^- + 5H^+$	$log\ K_3$
$\equiv S^sOH + Sn^{4+} + 5H_2O \leftrightarrow \equiv S^sOSn(OH)_5^{2-} + 6H^+$	$log\ K_4$
$Sn^{4+} + 4CO_3^{2-} \leftrightarrow Sn(CO_3)_4^{4-}$	$log\ K_5$
$Sn^{4+} + DOM\_s^- \leftrightarrow SnDOM\_s^{3+}$	$logK_s^{**(Sn-DOM)}$
$Sn^{4+} + DOM\_w^- \leftrightarrow SnDOM\_w^{3+}$	$logK_w^{**(Sn-DOM)}$
$Sn^{4+} + DOM^- \leftrightarrow SnDOM^{3+}$	$log\ K_6$
$Sn^{4+} + DOM\_s^- + \equiv S^sOH \leftrightarrow \equiv S^sOSnDOM\_s^{2+} + H^+$	$log\ K_7$
$Sn^{4+} + DOM\_w^- + \equiv S^sOH \leftrightarrow \equiv S^sOSnDOM\_w^{2+} + H^+$	$log\ K_8$

Table 9. Summary of the reactions and corresponding constants implemented in the different models used to describe the sorption experimental dataset on STx-1b

Model reference	Surface complexation constants $log\ K_1$ to $log\ K_4$	Strong site capacity $\equiv S^sOH$	Clay protolysis constants	Sn(IV)-carbonate complexation $log\ K_5$	Sn(IV)-BC DOM complexation
Model0_MoMo	Bradbury and Baeyens (2017)	Baeyens and Bradbury (1997)	Baeyens and Bradbury (1997)	/	/
Model1_MoMo	Bradbury and Baeyens (2017)	Baeyens and Bradbury (1997)	Thomas and Durce (2022b)	/	/

Table 10. Summary of the reactions and corresponding constants implemented in the different models used to describe the sorption experimental dataset on IdP. (1) recalculated from Durce et al. (2020b) using Equation (11).

Model reference	Surface complexation constants $log\ K_1$ to $log\ K_4$	Strong site capacity(2) $\equiv S^sOH$	Sn(IV)-carbonate complexation $log\ K_5$	Sn(IV)-BC DOM complexation	Dataset used for optimization
Model 0	Bradbury and Baeyens, 2009	Bradbury and Baeyens, 2009	/	/	
Model 1	Optimized on experimental data	Bradbury and Baeyens, 2009	/	/	Sorption edge and Sorption isotherm in $NaClO_4$ 0.017 M
Model 2	Optimized on experimental data	Optimized on experimental data	/	/	Sorption edge and Sorption isotherm in $NaClO_4$ 0.017 M
Model 3	from Model2	from Model 2	Optimized on experimental data	/	Sorption isotherm in $NaHCO_3$ 0.015 M
Model 4	from Model 2	from Model 2	/	$logK_s^{*(Sn-DOM)}$ / $logK_w^{*(Sn-DOM)}$ (1)	
Model 5	from Model 2	from Model 2	/	$logK_s^{**(Sn-DOM)}$ / $logK_w^{**(Sn-DOM)}$ (1) and $log\ K_{7/8}$ optimized on experimental data	Sorption isotherm in $NaClO_4$ 0.017 M + DOM_$NaClO_4$
Model 6	from Model 2	from Model 2	/	$log\ K_6$ optimized on experimental data	Sorption isotherm in $NaClO_4$ 0.017 M + DOM_$NaClO_4$
Model 7	from Model 2	from Model 2	/	/	
Model 8	from Model 2	from Model 2	from Model 3	/	

Table 11. Summary of the reactions and corresponding constants implemented in the component additivity models used to describe the sorption isotherm on BC. (1) recalculated to BC content of IdP (35 wt%)

Model reference	Surface complexation constants $log\ K_1$ to $log\ K_4$	Strong site capacity $\equiv S^sOH$	Sn(IV)-carbonate complexation $log\ K_5$	Sn(IV)-BC DOM complexation
Model_CA_1	from Model 2	from Model 2× 0.35(1)	/	/
Model_CA_2	from Model 2	from Model 2 × 0.35(1)	from Model 3	
Model_CA_3	from Model 2	from Model 2× 0.35(1)	from Model 3	$log\ K_6$ from Model 6
Model_CA_4	from Model 2	from Model 2× 0.35(1)	from Model 3	$log\ K_7$ and $log\ K_8$ from Model 5

2.6.2 Modelling of IdP datasets

2.6.2.1 Sorption edge and sorption isotherm in $NaClO_4$ 0.017 M

The 2SPNE SC model was optimized to describe the experimental data. Two options were considered: a sole optimization of the surface complexation constants ($log\ K_1$ to $log\ K_4$), referred to as 'Model 1', or a combined optimization of the surface complexation constants ($log\ K_1$ to $log\ K_4$) and of the strong site capacity ($n(\equiv S^sOH)$), referred to as 'Model 2'. In both cases, the constants, and the site capacity for Model 2, were optimized simultaneously on the sorption edge and sorption isotherm datasets. The experimental data and model were compared to the model reported by Bradbury and Baeyens (2009), which was implemented with the Sn(IV) surface complexation constants reported in Table 7, the IdP strong site capacity reported in Table B.1 of Appendix D and the Sn(IV) hydrolysis constants used by the authors and reported in Table B.3 of Appendix D. This model was referred to as 'Model 0'.

2.6.2.2 Sorption isotherm in $NaHCO_3$ 0.015 M

As previously discussed, Sn(IV) complexation constants with carbonate are not included in the Thermochimie V10a database. In a first modelling attempt, the effect of carbonate was neglected and the experimental sorption isotherm in $NaHCO_3$ 0.015 M was modelled using Model 2, i.e with the Sn optimized (IV) surface complexation constants and strong site capacity .
In a second step, the Sn(IV)-carbonate complexation was integrated in the model. Based on the sole isotherm dataset, it is not possible to identify which complexation reactions are taking place in our conditions, but an analogy with Zr(IV) can be made. Sn(IV) has indeed an ionic radius similar to Zr(IV) and could be expected to follow Zr(IV) geochemical behaviour. The formation of $Zr(CO_3)_4^{4-}$ and the corresponding constant (log K=42.9) were experimentally validated (Brown et al., 2008) and by analogy, it was chosen to write the Sn(IV)–carbonate complexation with the formation of $Sn(CO_3)_4^{4-}$:

$$Sn^{4+} + 4CO_3^{2-} \leftrightarrow Sn(CO_3)_4^{4-} \qquad log\ K_5 \qquad (8)$$

The corresponding complexation constant ($log\ K_5$) was optimized to fit the experimental sorption isotherm and the model was referred to as 'Model 3'.

2.6.2.3 Sorption isotherm in $NaClO_4$ 0.017 M in presence of BC DOM

In our previous work on Sn(IV), we measured the Sn(IV) complexation with BC DOM in present day BC conditions, i.e in $NaHCO_3$ 0.015 M and at a pH of 8.34 ± 0.08 (Durce et al., 2020a; Durce et al., 2020b). The complexation data were modelled using a 2-sites non-linear Langmuir isotherm by considering the following simple reactions:

$$Sn_{inorg} + DOM\_s \leftrightarrow SnDOM\_s \qquad \log K_s^{(Sn-DOM)} = 8.80 \qquad (9)$$

$$Sn_{inorg} + DOM\_w \leftrightarrow SnDOM\_w \qquad log\ K_w^{(Sn-DOM)} = 4.85 \qquad (10)$$

Where DOM_s and DOM_w would represent strong and weak binding sites present on BC DOM, respectively, and with a ratio of DOM_s/DOM_w = (1.06 ± 0.31) × 10^{-3}.
The exact nature and stoichiometry of the complexation reaction(s) couldn't be unravelled with the data in presence, but the determined constants were assumed to be a good representation of the level of binding in repository conditions.

Our previous experimental sets and the present work were performed at a close pH (8.34 vs 8.37) and ionic strength (0.015 vs 0.017 M), but in a different media ($NaHCO_3$ vs $NaClO_4$). The constants reported in Durce et al. (2020b) were recalculated taking into account the complexation with carbonate and the hydrolysis behaviour of Sn(IV) using Equation (11) and Equation (12).

$$logK_{s/w}{}^{**(Sn-DOM)} = logK_{s/w}{}^{(Sn-DOM)} + logA_s \quad (11)$$

$$A_s = 1 + \frac{K_{OH}^1}{[H^+]} + \frac{K_{OH}^2}{[H^+]^2} + \frac{K_{OH}^3}{[H^+]^3} + \frac{K_{OH}^4}{[H^+]^4} + \frac{K_{OH}^5}{[H^+]^5} + \frac{K_{OH}^6}{[H^+]^6} + [CO_3^{2-}]^4 \times K_5 \quad (12)$$

With A_s, the side reaction coefficient and $[CO_3^{2-}]$, the concentration of carbonate at the pH of Durce et al. (2020b) experiments estimated at 1.50 × 10^{-4} mol/L.
The values of the recalculated constants and of the side reaction coefficient are reported in Table 12.

Table 12. Side reaction coefficient and Sn(IV)-DOM complexation constants

$\boldsymbol{logA_s}$	41.2
$\boldsymbol{logK_s{}^{**(Sn-DOM)}}$	50.0
$\boldsymbol{logK_w{}^{**(Sn-DOM)}}$	46.0

The adapted model, referred to as 'Model 4' was based on Model 2 to which the sus-mentioned complexation reactions were added with the corresponding recalculated constants.

In a second modelling exercise, the model was adapted to better describe the experimental sorption of Sn(IV) in presence of DOM_$NaClO_4$. Two options were considered. One option was to implement the Langmuir isotherm reported by Durce et al. (2020b) with the recalculated complexation constants as reported in Table 12, but integrating also the sorption of the formed Sn(IV)-DOM complexes to the model. Simple 1:1 reactions were considered (Equations (13) and (14)) . The surface complexation constants for the two Sn(IV)-DOM complexes, SnDOM_s and SnDOM_w, were referred to as K_7 and K_8 and it was assumed that $K_7 = K_8$. The corresponding model was referred to as 'Model 5'

$$Sn^{4+} + DOM\_s^- + \equiv S^sOH - \leftrightarrow \equiv S^sOSnDOM\_s^{2+} + H^+ \qquad log\ K_7 \quad (13)$$

$$Sn^{4+} + DOM\_w^- + \equiv S^sOH - \leftrightarrow \equiv S^sOSnDOM\_w^{2+} + H^+ \qquad log\ K_8 \quad (14)$$

A second option was a simplified ligand model accounting for only one binding site on BC DOM. Sn(IV) complexation with BC DOM was, in that case, implemented with the reaction reported in Table 5 and the associated constant, $logK_6$:

$$Sn^{4+} + DOM^- - \leftrightarrow SnDOM^{3+} \qquad log\ K_6 \quad (15)$$

The corresponding complexation constant ($log\ K_6$) was optimized to fit the experimental sorption isotherm and the model is referred to as 'Model 6'.

2.6.2.4 Sorption isotherm in Synthetic Seawater

The effect of an increasing salinity on the sorption on clay material could result from a change of the contribution of cation exchange, the interlayers of the swelling clays tending to collapse with an increase of ionic strength. The electric double layer at the surface of the clay will also reduce and the increase of concentration of divalent cations could enhance the competition effect.
In the model put here forward for Sn(IV) sorption onto IdP, the contribution of cation exchange on Sn(IV) was neglected and not included as Sn(IV) strongly hydrolyses already from low pH. It is therefore expected that the collapsing of the clay sheet interlayers would not affect the sorption of Sn(IV).
Electrostatics are not integrated in the 2SPNE SC/CE model as it was showed previously by Bradbury and Baeyens (1997), that a model including an electrostatic term was unable to reproduce the experimental sorption data. Considering this postulate, the reduction of the electric double layer with the use of synthetic seawater is not expected to affect the Sn(IV) sorption onto IdP, or at least won't be taken into account in the model.
Regarding the competition effect with cations present in SSW, it is most likely negligible. On the one hand, Sn(IV) has a clearly different chemistry and hydrolysis behaviour than the divalent cations contained in SSW and the competition between them should be rather limited. Studies on competitive sorption onto clays indeed showed that competition tended to be selective and to occur only for elements with similar chemistry (Bradbury and Baeyens, 2005a; Fernandes et al., 2019; Soltermann et al., 2014b). On the other hand, the recent study published by Sugiura et al. (2021) showed that Ca^{2+} and Sr^{2+} would sorb on the weak sites rather than the strong sites of montmorillonite. By analogy, it is likely that the same behaviour

would occur with IdP. In our experimental conditions, Sn(IV) being sorbed on the strong sorption sites, it should not compete with the divalent cations of SSW, at least not with Ca^{2+} and Sr^{2+} and by analogy most likely also not with Mg^{2+}.

In a first modelling exercise, the contribution of Sn(IV)-carbonate complexation to the Sn(IV) sorption in SSW was neglected. The model used to describe the experimental sorption isotherm obtained in SSW, corresponded therefore to Model 2.

In a second modelling exercise, the Sn(IV)-carbonate complexation was taking into account assuming the same equation as used in section 2.6.2.2 and Model 3 was applied to the experimental data.

2.6.2.5 Modelling of sorption isotherm on BC in SPRING water

The modelling of Sn(IV) sorption onto BC is based on the component additive approach (section 2.1) and to be representative of the Boom Clay system it integrates the contribution of surface complexation on the 2:1 clay minerals, the aqueous complexation with the BC DOM present in solution and the aqueous complexation with carbonate dissolved in solution. To evaluate the contribution of each mechanism on the sorption of Sn(IV), the model is built in a stepwise manner, by gradually increasing its complexity.

In a first step, only the contribution of the surface complexation on the 2:1 clay minerals is integrated. The average concentration of 2:1 clay minerals in the sample used in this study was measured by XRD analysis to 35 wt% (see Table 13) This value accounts for illite concentration and illite/smectite mixed layer concentration. Marques Fernandes et al. (2015) showed that approximating the sorption behaviour of the illite/smectite layer to the one of pure illite led to a relatively good representation of the sorption of several elements onto two argillaceous rocks. Dähn et al. (2021) confirmed this result for Zn sorption at low sorbate concentration. In agreement with these two studies, it was assumed that Sn(IV) sorption onto the illite/smectite mixed layer present in BC had the same characteristics than on pure illite. The Sn(IV) sorption isotherm on BC was performed in SPRING water which contains various cationic/anionic species. The competitive sorption with the cations present in SSW was assumed negligible (section 2.6.2.4) and the same was done for SPRING water. The complexation of Sn(IV) with some inorganic anions present in SPRING water such as sulfate could partly control its aqueous speciation and affect its sorption. However, the concentration of sulfate in SPRING water was reported to be low, < 5 mg/L (De Craen et al., 2004; Durce et al., 2015), and should therefore not significantly affect the Sn(IV) speciation. For simplicity, SPRING water composition was therefore approximated to a solution of $NaHCO_3$ 0.015 M.
The optimized strong site capacity of Model 2, was adapted to account for the 35 wt% of pseudo-illite in BC and the resulting model is referred to as 'Model_CA_1'.

In a second step, Model_CA_1 was adapted to take into account the role of Sn(IV)-carbonate complexation. The complexation reaction with the complexation constant of Model 3 (section 2.6.2.2) was added to Model_CA_1 and the resulting model is referred to as 'Model_CA_2'.

In a third step, Sn(IV)–DOM complexation and the potential formation of DOM–Sn(IV)-BC complexes were added to the model. On the one hand, Model_CA_2 was adapted to take into account the role of Sn(IV)-BC DOM complexation in the Sn(IV) sorption onto BC. SPRING water contains 82 ± 25 ppm of DOC (section 2.3.3) which translates to (8.77 ± 3.18) × 10^{-4} mol/L considering the PEC_{eff} reported by Durce et al. (2020b) and taken here as reference (section 2.3.4). DOM in SPRING water is different than DOM_$NaClO_4$ as it contains a large fraction of small molecules (< 1 kDa, Durce et al. (2015)) which have been filtered out during the extraction of DOM_$NaClO_4$. It was however considered for this modelling exercise that DOM_$NaClO_4$ and the DOM present in SPRING water display the same complexation properties with respect to Sn(IV). Model_CA_2 was therefore adapted to integrate the complexation reaction with the complexation constant of Model 6 (section. 2.6.2.3). The resulting model is referred to as 'Model_CA_3'. On the other hand, Model_CA_2 was adapted to take into account the role of Sn(IV)-BC DOM complexation and of the sorption of the formed complexes. The aqueous Sn(IV)–DOM complexation was described with the constants $logK_s^{**(Sn-DOM)}$ and $logK_w^{**(Sn-DOM)}$ and the sorption of the formed complexes was added to the model with the optimized constants *log* K_7 and *log* K_8. The resulting model is referred to as 'Model_CA_4'.

3 Results and discussion

All the experimental uncertainties are given as 2σ or 2 standard deviation (SD) (95% confidence intervals).

3.1 Characterisation of the clay minerals and Boom Clay

3.1.1 Mineralogy

The semi-quantitative XRD analyses showed that after purification the montmorillonite STx-1b was almost completely pure, with a trace amount of quartz evidenced by a small peak at 26.6°2. The IdP sample was found to be intermixed with K-feldspar, in an estimated amount of 10 wt.%. No other impurities could be detected. The XRD diffractogram of both clay samples are reported in Appendix G.
The results of the quantitative XRD analyses of the two BC core subsamples are reported in Table 13. As it can be seen, the two samples display a different composition with subsample 2 enriched in clay compared to subsample 1. The average composition is taken as reference, since we cannot distinguish which of the subsamples is more representative of the sample used here for the sorption experiments.

Table 13. Composition of subsamples of the BC core measured by XRD and their average.

	Subsample 1 (wt%)	Subsample 2 (wt%)	Average (wt% ± range)
Plagioclase	2	1	1.5 ± 0.5
Calcite	0.5	0.9	0.7 ± 0.2
Pyrite	2	1	1.5 ± 0.5
Anatase	1	0.8	0.9 ± 0.1
K-feldspar	7	5	6 ± 1
Quartz	42	27	34.5 ± 7.5
SUM Non-Clay	**54**	**36**	**45± 9**
Kaolinite	6	10	8 ± 2
2:1 Al Clay	31	39	**35 ± 4**
Chlorite	0	3	1.5 ± 1.5
Muscovite	9	12	10.5 ± 1.5
SUM Clay	**46**	**64**	**55 ± 9**

3.1.2 TOC-TIC content

The TIC and TOC content of IdP and STx-1b was not measured as the two clays are assumed free of organic and inorganic carbon. The TIC and TOC of the BC samples were measured respectively to 0.11 ± 0.03 and 1.23 ± 0.03 mg/kg. These corresponds to the average of the measurements of the two subsamples taken from the BC core with the twice the standard deviation over all the analyses.

3.1.3 Reactivity

3.1.3.1 Specific surface area via N_2-adsorption

The calculated surface areas of the IdP, STx-1b and BC samples are reported in Table 14. For more details, we refer the reader to the analysis reports provided in the electronic supplement.

Table 14. BET surface area. The measurement error is fixed as 2σ=10%

Samples	BET Surface Area (m^2/g)
IdP	115 ± 12
STx-1b	124 ± 12
BC	47 ± 5

IdP and STx-1b display similar surface areas, while the surface area of BC is less than half. This is consistent with the mineralogy of BC, which is not solely composed of clay minerals (Table 13).

3.1.3.2 Site capacities via potentiometric titrations

The potentiometric titrations were performed on IdP and STx-1b according to the protocol reported by Thomas and Durce (2022a). The titration of the BC was however not performed in that work.
The experimental results of the titrations are reported in Thomas and Durce (2022b). Only the main results and conclusions are reported here.
The offline potentiometric titrations of IdP in $NaClO_4$ 0.015 M corrected by the online titrations of the equilibrium solutions and by the consideration of clay dissolution and cation exchange gave a titration curve slightly different from the one reported by Bradbury and Baeyens (2009). The difference was confirmed when the data were modelled using the protolysis constants and site capacities of the same authors and reported here in Appendix D. However, the difference was judged as minimal and it was concluded that the protolysis constants and site capacities of Bradbury and Baeyens (2009) were valid for our batch of IdP.
The titration results obtained on STx-1b following the same protocol and corrections as applied for IdP, showed a strong deviation from the results reported by Baeyens and Bradbury (1997). This was clearly evidenced when the data were modelled using the protolysis constants and site capacities in Bradbury and Baeyens (1997) and reported here in Appendix D. To describe the experimental data, both the protolysis constants and the sites capacities had to be adapted to the values summarized in Table 15. Thomas and Durce (2022b) attributed the differences with Baeyens and Bradbury (1997) and Bradbury and Baeyens (1997) to the different source of Montmorillonite used by the latter who used the SWy-1 Montmorillonite. However, Thomas and Durce (2022b) also mentioned that performing extra potentiometric titrations would be pertinent to gain more confidence in their results.

Table 15. Surface site capacities and protolysis constants for the STx-1b as reported by Thomas and Durce (2022b)

	Montmorillonite STx-1b
$\equiv S^{w1}OH + H^+ \leftrightarrow \equiv S^{w1}OH^{2+}$	$log\ K$= 4.5
$\equiv S^{w2}OH + H^+ \leftrightarrow \equiv S^{w2}OH^{2+}$	$log\ K$ = 4.5
$\equiv S^{s}OH + H^+ \leftrightarrow \equiv S^{s}OH^{2+}$	$log\ K$ = 4.5
$\equiv S^{w1}OH \leftrightarrow \equiv S^{w1}O^- + H^+$	$log\ K$ = -7.9
$\equiv S^{w2}OH \leftrightarrow \equiv S^{w2}O^- + H^+$	$log\ K$ = -10.5
$\equiv S^{s}OH \leftrightarrow \equiv S^{s}O^- + H^+$	$log\ K$ = -7.9
$\equiv S^{w1}OH$	$Capacity = 5.2 \times 10^{-2}$ mol/kg
$\equiv S^{w2}OH$	$Capacity = 5.2 \times 10^{-2}$ mol/kg
$\equiv S^{s}OH$	$Capacity = 2.6 \times 10^{-3}$ mol/kg

3.1.4 Clay equilibrium solutions

The cationic and anionic composition of the solutions in equilibrium with the clay suspensions at ~20 g/L are reported in Table C.2 and Table C.3 of Appendix C. Both IdP and BC suspensions contained a significative amount of metals that could compete with Sn(IV) for sorption. However, Sn(IV) has a different chemistry and hydrolysis behaviour than the metals contained in the suspensions (mainly divalent) and it is assumed that the competition between them was rather limited. Consequently, the elements detected in the suspension were not integrated in the modelling. The measured concentration of natural Sn in the suspensions was (6.01 ± 1) × 10^{-9} and (2.05 ± 0.2) × 10^{-8} mol/L in IdP_0 and BC_1, respectively. It was below detection limit in IdP_1. The concentration measured in IdP_0 was also close to detection limit and outside the calibration range. Considering the relatively low value and its large uncertainty, the concentration of natural Sn in the IdP sorption experiments was assumed negligible. In the case of the blank BC suspensions, the average natural Sn concentration measured in the equilibrium solution was (5.50 ± 0.24) × 10^{-9} mol/L. This was measured with a lower detection limit than IdP_0 (lower dilution) and the value is assumed reliable. The measured natural Sn concentration in the BC blank samples is further taken into account when reporting the experimental results of the sorption experiments performed on BC.

3.2 Sorption of Sn(IV) onto pure clay minerals in $NaClO_4$ 0.017 M

3.2.1 Sorption edge and sorption isotherm onto IdP

The experimental sorption edge and sorption isotherm of Sn(IV) on IdP in $NaClO_4$ 0.017 M are reported in Figure 2 and in Figure 3, respectively, together with the results of the three models, Model 0, Model 1 and Model 2.
The sorption of Sn(IV) on IdP is very strong over the full range of pH. The experimental sorption edge does not show a strong 'edge' in agreement with the hydrolysis of Sn(IV) occurring already at low pH. The decrease of sorption at low pH, i.e below

pH 4, confirms the low contribution of cationic exchange. On the other side of the pH range, the clear decrease of sorption at pH > 10 results from the predominance of $Sn(OH)_6^{2-}$ and its low sorption affinity on the negatively charged IdP.

Model 0 corresponds to the 2SPNE SC model proposed by Bradbury and Baeyens (2009) to describe their Sn(IV) sorption edge on IdP. The sorption of Sn(IV) measured here is consistently lower than reported by the authors. Over the range of pH, our log K_d values are lower from 0.2 to 1.0 log than predicted with Model 0.

The experimental protocol followed by Bradbury and Baeyens (2009) is not reported in details and the existence of experimental artefacts such as side sorption on tubes cannot be ruled out. The sorption of Sn(IV) on the tube walls was indeed found significant at all pH-values (up to 91%) in the blank experiments. However by measuring the activities of the suspensions just before centrifugation (see section 2.5),the bias due to Sn(IV) side sorption on tubes is expected limited The measured activities were taken as Sn_0 in Equation (7). The calculated loss of Sn in the blanks in the different experiments as reported in Appendix E, did not show any strong artefact coming from the centrifugation step. At pH~8.4, as used for the sorption isotherms, most of the measurements, revealed a Sn loss below 10 % during the centrifugation step. A stronger loss was observed at lower pH with in average a fraction of 0.52 ± 0.07 of Sn that was removed at pH < 7 from the blank solutions of the edge experiments. This result remained unexplained and though the bias could be smaller in presence of the clays, one should keep in mind that the sorption on both IdP and STx-1b could be here slightly overestimated at pH < 7.
The experiments performed in the present work and by Bradbury and Baeyens (2009) were performed at a different ionic strength, 0.1 vs 0.017 M, and in case of a strong involvement of cation exchange in the sorption, this could affect the obtained sorption edges. This is however not expected in the case of Sn(IV), especially as it would lead to an opposite trend to the one observed here, i.e higher sorption at lower ionic strength, and would have an effect mostly on the low pH range. At pH 8.56 at which the sorption isotherm was obtained, the sorption is mainly dominated by surface complexation with a negligible contribution of cation exchange mechanism, especially in the case of Sn(IV). Hence, the effect of ionic strength on the results should be minimal.
Regarding the experimental protocol, Bradbury and Baeyens (2009), used significantly 'harsher' centrifugation conditions (up to 108 800 × g for 1 h) than in the present study. On the one hand the settling of possible Sn(IV) colloids could artificially increase the log R_d values. On the other hand, it could also have ensured a better separation of the smallest clay particles from the solution. Based on the estimated clay density, we calculated that the centrifugation conditions applied here (20 000 × g for 1 h) should remove clay particles > 20 nm which should be sufficient to the settling of the IdP particles. It is however possible that a fraction of the smallest IdP particles did not settle, apparently lowering the Sn(IV) sorption. However, without a thorough study on the effect of centrifugation on the measured $log\ R_d$ values and considering the lack of information on the experiments performed by Bradbury and Baeyens (2009), it is difficult to conclude on the influence of phase separation conditions.

The batch of IdP used in the present work was prepared during the CatClay project (Altmann et al., 2015) and could be slightly different from the one used by Bradbury and Baeyens (2009). This could affect the clay properties with respect to sorption. The sorption site capacities and hydrolysis constants of IdP were not remeasured during CatClay. However, the measured CEC was found to be smaller than reported by Bradbury and Baeyens (2009) (190 ± 10 vs 225 ± 15 meq/g) indicating the existence of some differences between the two batches.

As discussed in the Modelling section, the Sn(IV) hydrolysis constants reported by Bradbury and Baeyens (2009) differ from those validated by NEA (Gamsjäger et al., 2012) and those integrated in the Thermochimie database. In their work on Montmorillonite (Bradbury and Baeyens, 2005b), the authors reported the need to integrate the first three hydrolysis species to properly describe their experimental sorption edge. The same is observed here and it appears that with considering only the four, fifth and sixth hydrolysis as present in the Thermochimie database and despite an optimisation of the Sn(IV) surface complexation constants (Model 1) the high sorption observed at low pH is not well reproduced.
The apparent strong sorption could imply the involvement of the sorption of $Sn(OH)^{3+}$, $Sn(OH)_2^{2+}$ and $Sn(OH)_3^{+}$ as suggested by Bradbury and Baeyens (2009) or could be (partially) the result of Sn(IV) precipitation as suggested by the blank experiments. Although, the use of the constant in the Thermochimie database was not able to properly describe the experimental data obtained at low pH, it satisfactorily depicted the sorption of Sn(IV) for pH > 7. These pH conditions being the most relevant for Boom Clay and the Thermochimie Sn(IV) constants being assumed the most reliable, it was decided to keep using them for all the modelling exercises.
As visible on the experimental sorption isotherm, sorption is linear until an equilibrium Sn(IV) concentration of 1.6×10^{-9} mol/L over which the distribution coefficient (R_d) starts to decrease indicating a possible site saturation. The results do not clearly evidence the dual sorption of Sn(IV) on two different sites. At the low Sn(IV) concentration used here, it can indeed be expected that the interaction of Sn(IV) with the 'strong' sites of IdP dominates the sorption. The low contribution of sorption on the IdP weak type of sites at the investigated concentration impedes to extract information on the sorption behaviour of Sn(IV) on those sites, which could dominate at higher concentration. Though not essential in a context of nuclear waste repository where only radionuclide trace concentrations might be expected, it could be interesting to extend the working range of Sn(IV) concentration until precipitation to evaluate the sorption behaviour of this element on the weak

sites of IdP. Model 1 allows a good description of the sorption at low Sn(IV) concentration, but it fails in describing the apparent site saturation observed at Sn(IV) equilibrium concentration > 1.6×10^{-9} mol/L.

Allowing the strong site capacity to be optimized along with the surface complexation constants as in Model 2, improves the fit of the experimental isotherm (Figure 3). However, the optimized strong site sorption capacity (Table 16) had to be reduced by a factor two in comparison to the values reported by Bradbury and Baeyens (2009) (Appendix D). A variation of the sorption site capacity can be expected from IdP batch to batch. However as discussed in section 3.1.3.2, the results of the potentiometric titration performed by Thomas and Durce (2022b) on the IdP batch used in this work, did not show a strong deviation from the results reported by Bradbury and Baeyens (2009). Both the hydrolysis constants and the site capacity for the 'weak sites' were assumed similar than reported by Bradbury and Baeyens (2009). The potentiometric titrations do not provide direct information on the strong sites and the strong site capacity was determined by Bradbury and Baeyens (2009) on sorption data. This results in a higher uncertainty on the properties of these sites. Such a reduction of the site capacity was not reported in the modelling exercises performed in the context of Catclay (Altmann et al., 2015), for which the same IdP batch was used as here. However, only divalent and trivalent elements were investigated in the frame of the project and the strong hydrolysis of Sn(IV) could prevent it gaining access to the totality of the IdP strong sorption sites.

We can conclude that, most likely, the difference between the results obtained previously by Bradbury and Baeyens (2009) and the results of the present study is due to a combination of factors involving experimental artefacts, different experimental conditions and/or protocol and heterogeneity of IdP. However, none of these factors evidently stood out as a main contributor. The modelled reduction of strong sorption site capacity was not confirmed by any other extra experimental means. It however clearly provides a better description of our experimental data and it was in consequence assumed to be a relevant assumption. Model 2 is therefore taken as a reference for all further modelling.

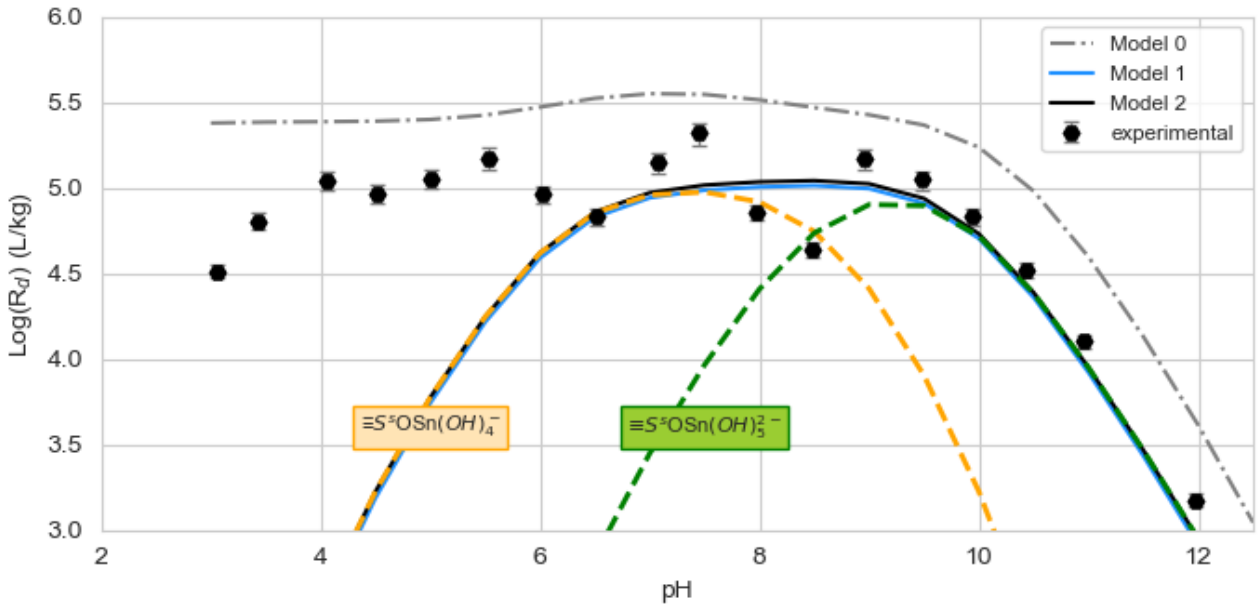

Figure 2. Sn(IV) sorption edge on IdP in $NaClO_4$ 0.017 M, experimental and modelling results.

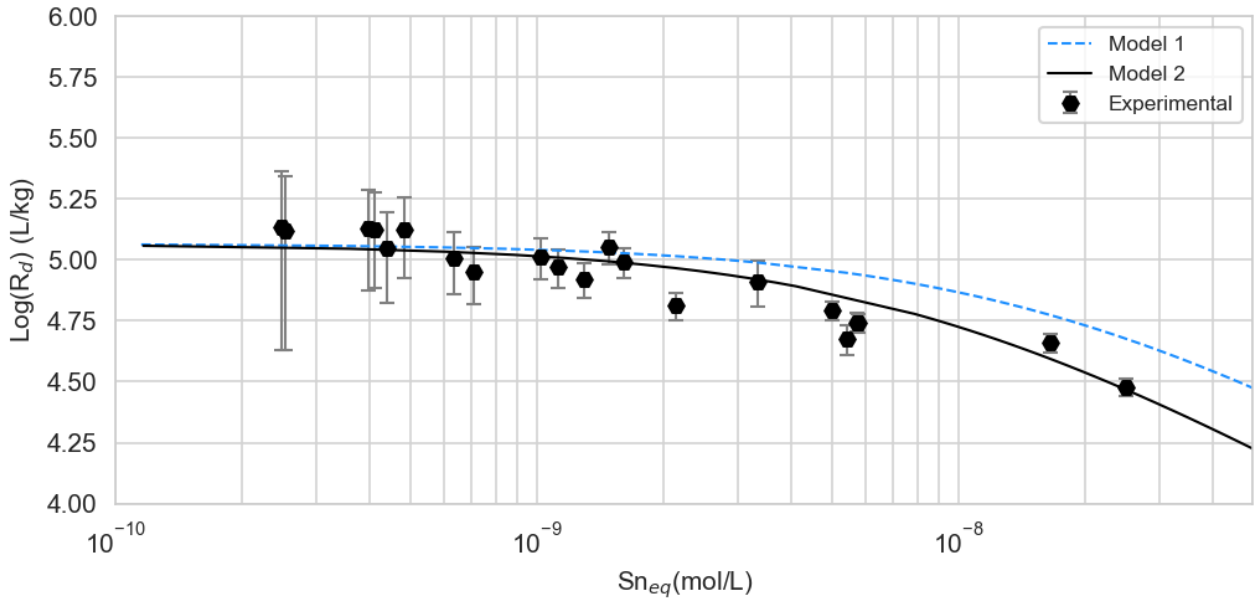

Figure 3. Sn(IV) sorption isotherm on IdP in $NaClO_4$ 0.017 M at pH 8.56 ± 0.05, experimental and modelling results.

Table 16. Optimized parameter values. The values given in brackets correspond to the confidence interval (1) provided by the UCode software and (2) estimated from the sensitivity analysis as reported in Durce et al. (2022)

Parameters	Opimized value	Model and dataset used for optimization
$log\ K_3$	9.1 [8.9-9.2] (1)	Model 1 Sorption Edge and Sorption Isotherm in $NaClO_4$ 0.017 M
	9.4 [8.8-10.1] (2)	Model 2 Sorption Edge and Sorption Isotherm in $NaClO_4$ 0.017 M
$log\ K_4$	0.55 [0.42-0.69] (1)	Model 1 Sorption Edge and Sorption Isotherm in $NaClO_4$ 0.017 M
	0.9 [0.7-1.4] (2)	Model 2 Sorption Edge and Sorption Isotherm in $NaClO_4$ 0.017 M
$log\ K_5$	**55.8** [55.7-56.1] (2)	Model 3 Sorption Isotherm in $NaHCO_3$ 0.015 M
$log\ K_6$	**45.4** [45.2-46.0] (2)	Model 6 Sorption Isotherm in $NaClO_4$ 0.017 M + DOM_$NaClO_4$
$log\ K_7$	**48.9** [48.5-49.4] (2)	Model 5 Sorption Isotherm in $NaClO_4$ 0.017 M + DOM_$NaClO_4$
$log\ K_8$	**48.9** [48.5-49.4] (2)	Model 5 Sorption Isotherm in $NaClO_4$ 0.017 M + DOM_$NaClO_4$
$\equiv S^sOH\ capacity$ (mol/kg)	**1.0×10^{-3}** [0.97-1.1] × 10^{-3} (2)	Model 2 Sorption Edge and Sorption Isotherm in $NaClO_4$ 0.017 M

3.2.2 Sorption edge and sorption isotherm onto STx-1b and effect of the S/L ratio

The experimental sorption edge and sorption isotherm of Sn(IV) on STx-1b in $NaClO_4$ 0.017 M are reported in Figure 4 and in Figure 5, respectively, together with the results of the two tested models, Model0_MoMo and Model1_MoMo.

As observed for IdP, Sn(IV) undergoes a strong uptake on STx-1b over the investigated range of pH and concentrations. The experimental sorption edge shows a flat profile until pH 6-7. The uptake softly decreases from pH 6-7 to 10 and a sharp

drop of sorption is observed at pH > 10. The drop of sorption at high pH is consistent with the results obtained on IdP and with the speciation of Sn(IV) which is dominated by $Sn(OH)_6^{2-}$ and $Sn(OH)_5^-$ considering the hydrolysis constant used by Bradbury and Baeyens (2009). Model0_MoMo and Model1_MoMo both based on Bradbury and Baeyens (2017) Sn(IV) surface complexation and hydrolysis constants show a similar pattern than the experimental results though it predicts a sharp decrease of sorption from already pH 8 where we observed a more progressive sorption decrease from pH 6-7 to pH 10.

As observed for IdP, the sorption of Sn(IV) measured here is consistently lower than reported by Bradbury and Baeyens (2005b) and Bradbury and Baeyens (2017) over the range of pH. The difference is even more marked than for IdP and is confirmed on the sorption isotherm, if one assumes that the model of Bradbury and Baeyens (2017) is valid over the range of Sn(IV) concentration investigated. The same arguments as proposed in the previous section for IdP could be discussed here. Two different sources of montmorillonite were used, Bradbury and Baeyens (2005b) used the Wyoming (SWy-1) montmorillonite, while the Texas STx-1b montmorillonite was used in the present work. As previously discussed in section 2.1.2, these two clays display some differences and the potentiometric titrations evidenced a different hydrolysis behaviour and sorption capacity. Yet, Model1_MoMo which uses the results of the STx-1b potentiometric titration does not provide a better description of the experimental data, it actually worsens it. The fact that a similar trend is observed for both the IdP and Montmorillonite systems suggest that 1/ differences in experimental conditions or protocols could play a role or 2/ Sn(IV) does not have access to the total capacity of strong sorption sites present on the clays as put forward by the modelling of the IdP sorption isotherm. But as already discussed, without a strict comparison of the used protocols and extra investigations, it is difficult to conclude.

The experimental sorption isotherm shows two plateaus at two different $log\ R_d$ values for the two solid/liquid ratios. The difference in average $log\ R_d$ values between the two plateaus is limited (5.04 ± 0.12 vs 4.40 ± 0.05 for a solid/liquid ratio of 0.10 and 0.50 g/L, respectively), but significative with respect to the experimental errors. The same influence of the solid/liquid ratio is also found in other investigated conditions (Figure 8 and Figure 10).
To confirm the dependence of sorption on the solid/liquid ratio, experiments were performed at different solid/liquid ratios in $NaClO_4$ 0.017 M (see section 2.5.4) and the results are reported in Figure 6. The two experimental sets give slightly different results, but in both cases a linear relationship between $log\ R_d$ and $log(S/L)$ is observed. Similar results were reported by W.Oscarson and B.Hume (1998) and other studies cited by the authors. The authors proposed two hypotheses to explain their results. On the one hand, the site accessibility could be impeded by particle-particle interaction with an increase of the solid/liquid ratio. On the other hand, the efficiency of centrifugation could decrease with an increase of the solid/liquid ratio leaving more clay particles in suspension and artificially decreasing the sorption. The results of W.Oscarson and B.Hume (1998) suggested that in their study, particle-particle interaction was most likely the cause of the decreasing R_d values. Our results showed no effect of the solid/liquid ratio on the Sn(IV) sorption onto IdP, but the purified STx-1b shows a different consistence and is certainly showing a different behaviour with an increase of solid/liquid ratio. The sorption of Sn(IV) is observed to be dependent on the solid/liquid ratio for all the investigated conditions, except in SSW (Figure 12). The higher ionic strength and higher concentration of divalent ions in SSW is likely to favour aggregation of the clay more than its dispersion. The absence of the solid/liquid ratio effect in these conditions would therefore tend to validate the second hypothesis, i.e a decrease of centrifugation efficiency with an increase of solid/liquid ratio more than particle-particle interaction. The results obtained at higher solid/liquid ratio would in consequence be less trustable. However, without a rigorous investigation on the efficiency of centrifugation at different solid/liquid ratio, which would require high speed centrifugation, it is not possible to confirm or infirm this hypothesis.

Another option could be that the effect of the solid/liquid ratio on the Sn(IV) sorption onto STx-1b is the result of competitive sorption with the cations released in solution by the STx-1b particles. The cationic composition of the equilibrium solutions measured at different solid/liquid ratios is reported into Table C.3 of the Appendix C. The change of the concentration of elements possibly competing with Sn(IV) for sorption does not show a clear trend with the solid/liquid ratio. This could be due to the heterogeneity of the clay or for some elements to a solubility or cation-exchange controlled release. In any case based on these results, it is difficult to highlight a possible involvement of competitive sorption in the observed solid/liquid ratio effect.

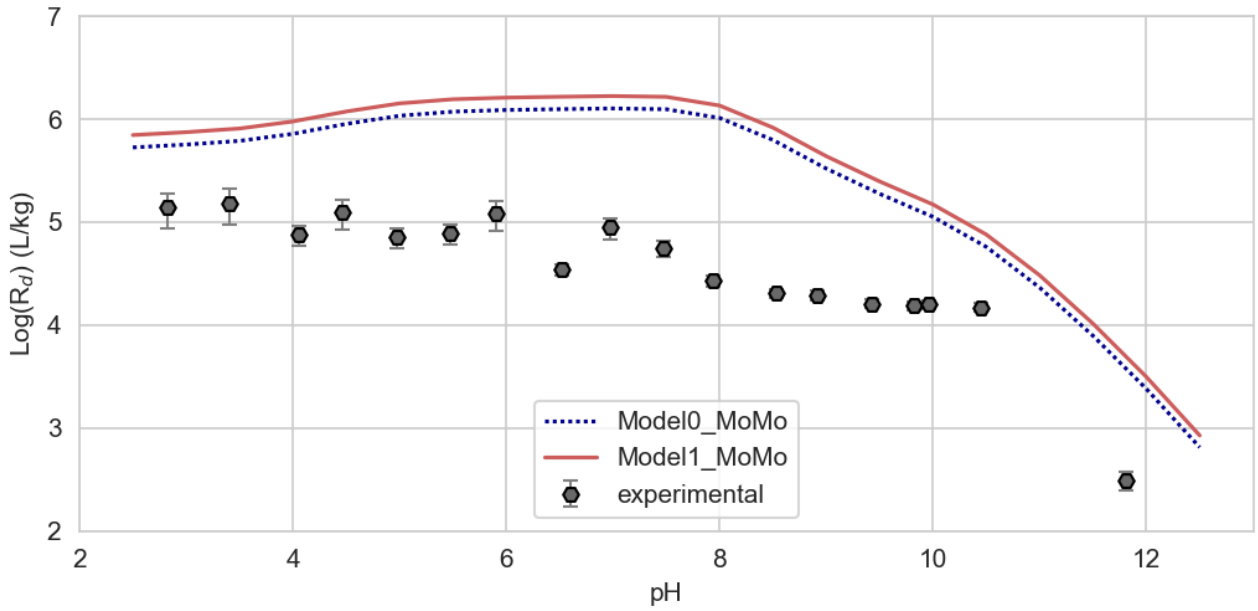

Figure 4. Sn(IV) sorption edge on STx-1b in $NaClO_4$ 0.017 M, experimental and modelling results

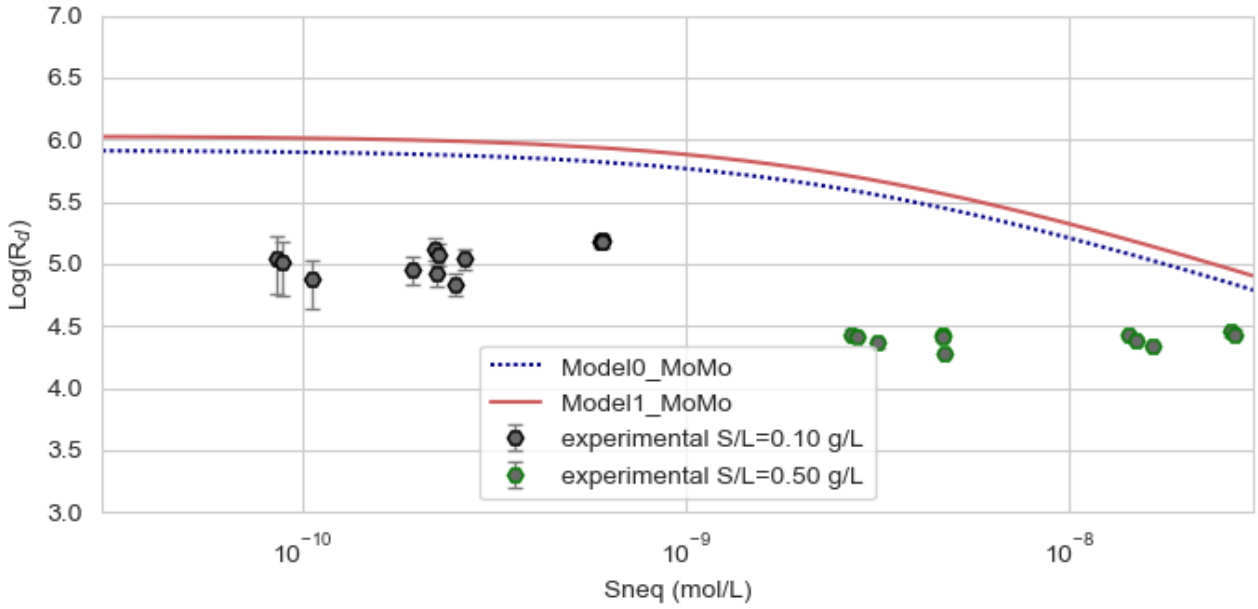

Figure 5. Sn(IV) sorption isotherm on STx-1b in $NaClO_4$ 0.017 M at pH 8.31 ± 0.03, experimental and modelling results

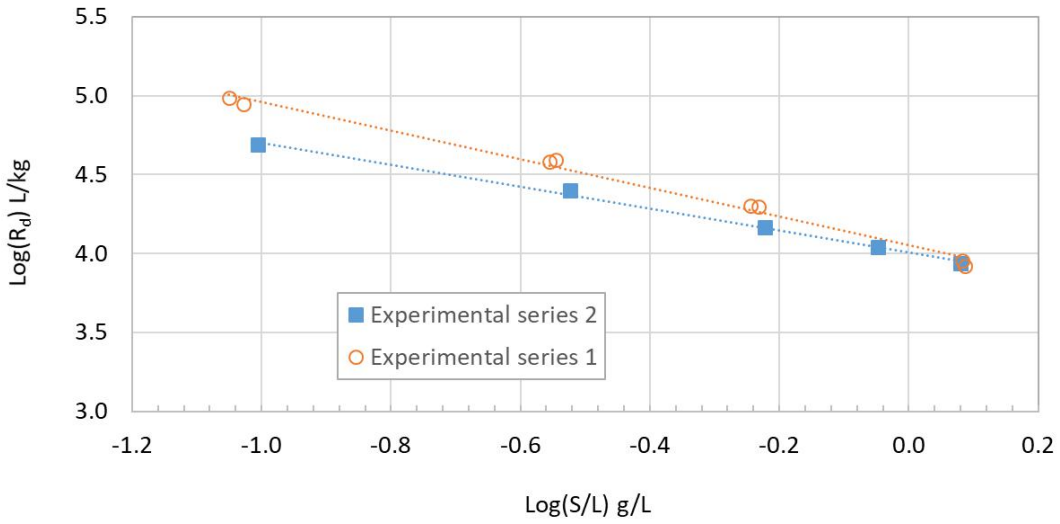

Figure 6. Sorption of Sn(IV) on STx-1b as a function of the solid/liquid ratio

3.3 Sorption of Sn(IV) onto pure clay minerals in presence of carbonate

3.3.1 Sorption isotherm onto IdP

The experimental sorption isotherm of Sn(IV) on IdP in $NaHCO_3$ 0.015 M is reported in Figure 7, together with the results obtained in $NaClO_4$ and the two models, Model 2 and Model 3.

The presence of carbonate slightly reduces the sorption of Sn(IV) on IdP in comparison to the $NaClO_4$ system. The resulting decrease of the $log\ K_d$ values remains small and does not exceed 0.3 log unit, but it is consistent over the full range of investigated concentrations. It is, however, within the commonly accepted error range of ± 0.2-0.5 log unit for log K_d values (Baeyens and Bradbury, 1997; Bradbury and Baeyens, 2005b). In the present conditions, the significance of the carbonate effect on Sn(IV) complexation is therefore highly dependent on the values taken for the experimental errors.

The integration of the complexation of Sn(IV) with carbonates in Model 3 with the optimized constant ($log\ K_5$) as reported in Table 16 provides a good description of the experimental points. Yet, as already discussed, the nature and the stoichiometry of the complexation reaction is unknown and the reaction (8) together with the value of $log\ K_5$ should be considered more as fit parameters than physical parameters. Nevertheless, if one considers the sorption reduction as significant, the Sn(IV) complexed to the carbonates would represent 39 % of the total aqueous Sn(IV) in the investigated conditions, which would be significantly higher than for Zr(IV) and show the importance of carbonate in the Sn(IV) speciation. Yet, extra experiments performed at different carbonate concentrations and at different pH would be required to confirm the results and to gain more information on the nature of the complexation reactions.

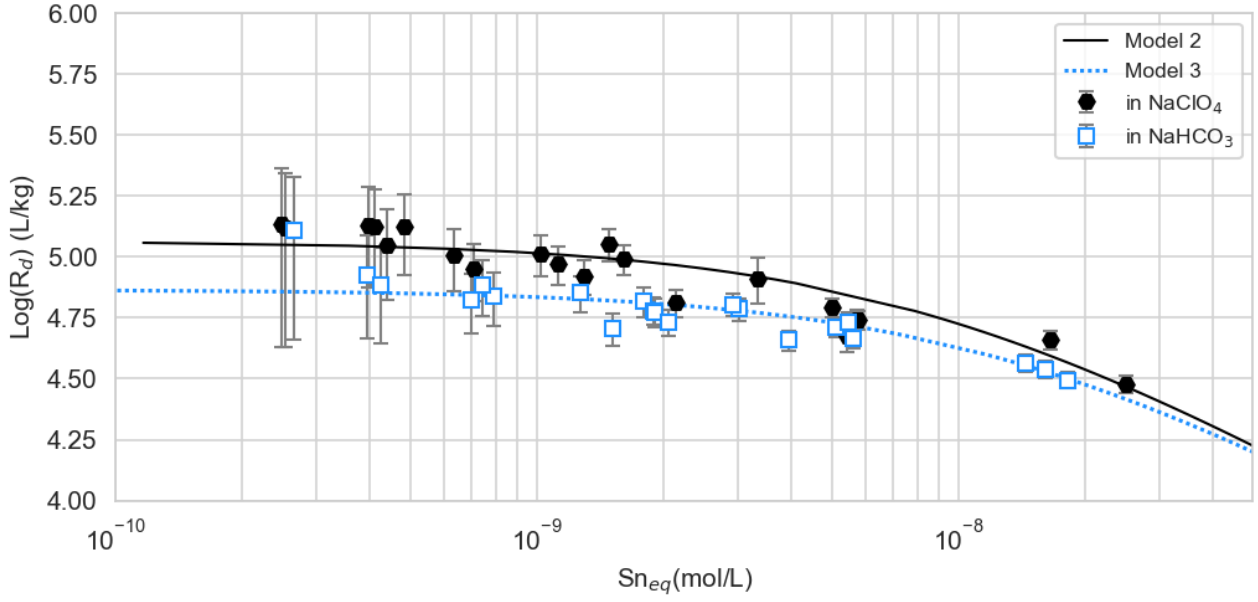

Figure 7. Sn(IV) sorption isotherm on IdP in $NaHCO_3$ 0.015 M and in $NaClO_4$ 0.017 M , experimental and modelling results

3.3.2 Sorption isotherm onto STx-1b

The experimental sorption isotherm of Sn(IV) on STx-1b in $NaHCO_3$ 0.015 M is reported in Figure 8, together with the results obtained in $NaClO_4$ 0.017 M.

As previously discussed, different results are obtained with different solid/liquid ratios. At a solid-liquid ratio of 0.10 g/L, the presence of carbonate could slightly reduce the sorption with an average $log\ R_d$ of 4.85 ± 0.08 in comparison to 5.04 ± 0.11 for the $NaClO_4$ 0.017 M. However, the decrease is small and within the data dispersion and experimental errors and so not obviously significant. At a higher solid-liquid ratio, the effect of carbonate on the sorption is not visible and the $log\ R_d$ values in $NaHCO_3$ and $NaClO_4$ are comparable, though it is not clear why carbonate would play a different role at different solid/liquid ratios.

The value of $log\ K_5$ determined in the IdP system would translate to the formation of 45 % of $Sn(OH)_3CO_3^-$ in $NaHCO_3$ 0.015 M and at the pH of the experiments (8.51) and so reduce the sorption accordingly in comparison to the $NaClO_4$ system. The resulting average $log\ R_d$ values for each solid-ratio are reported in blue and green in Figure 8. As it can be seen, at the lowest solid-liquid ratio, it matches well the experimental data points measured in $NaHCO_3$ 0.015 M. It however overestimates the effect of Sn(IV)-carbonate complexation at higher solid/liquid ratio at which no effect on sorption of the carbonate was observed.

Due to data dispersion and different results at different solid/liquid, it is not possible to conclude on the existence of a carbonate effect on the Sn(IV) sorption on STx-1b. Extra experiments would be required at higher carbonate content to overcome the data dispersion and the experimental uncertainty and validate the results.

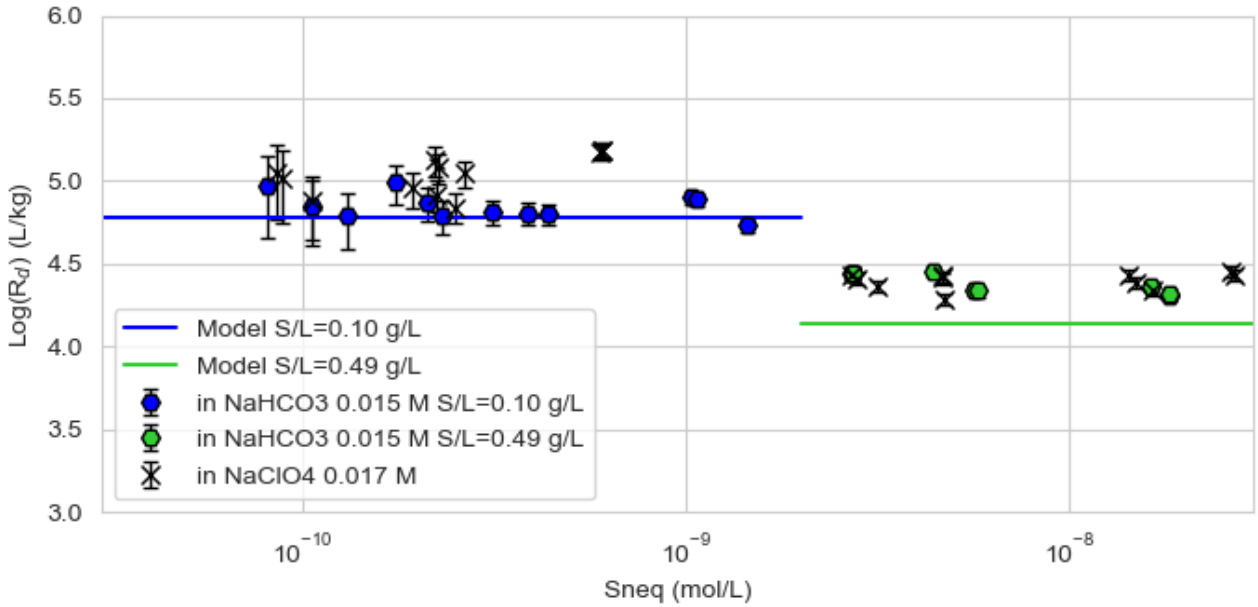

Figure 8. Sn(IV) sorption isotherm on STx-1b in $NaHCO_3$ 0.015 M at pH 8.51 ± 0.02. The green and blue lines correspond to the average calculated $log\ K_{d(NaHCO3)}$ such as $log\ K_{d(NaHCO3)} = log\ (K_{d(NaClO4)} \times (1 - 0.45))$

3.4 Sorption of Sn(IV) onto pure clay minerals in presence of BC DOM

3.4.1 Sorption isotherm onto IdP

The experimental sorption isotherm of Sn(IV) on IdP in 0.017 M $NaClO_4$ in presence of DOM_$NaClO_4$ is reported in Figure 9, together with the results obtained in pure $NaClO_4$ and with the three models, Model 4, Model 5 and Model 6.

As shown from the experimental data, the presence of BC DOM clearly reduces the sorption of Sn(IV) on IdP over most of the range of investigated concentrations with a decrease in $log\ R_d$ of up to 0.5 log unit.

The strong complexation of Sn(IV) with BC DOM was evidenced in Durce et al. (2020b) and was shown to depend on the loading, i.e the DOM/Sn(IV) ratio. A two-site Langmuir isotherm type model was used to fit the experimental data. The use of the determined constants (Table 12) recalculated taking into account the Sn(IV) hydrolysis constants and carbonate complexation in Model 4 significantly overestimates the sorption reduction measured here in presence of BC DOM. A comparison of the experimental data and the prediction of Model 4 also suggests the absence of two active complexation sites on the used BC DOM. At high Sn(IV) concentrations, the saturation of a strong complexation site of high affinity but low capacity on BC DOM as described by Durce et al. (2020b) would indeed limit the Sn(IV)-DOM concentration and increase the distribution coefficient of Sn(IV) on IdP, which is not observed experimentally.

The apparent lower effect of BC DOM on the Sn(IV) sorption on IdP than predicted using the data reported by Durce et al. (2020b) could be due to the use of different BC DOM batches. The BC DOM used by Durce et al. (2020b) was extracted following the same protocol as here (section 2.3.4), but it was redissolved in $NaHCO_3$ 0.015 M instead of $NaClO_4$ 0.017 M. The PEC_{eff} of the batch used in the present work was not measured, but was assumed equal to the PEC_{eff} measured by Durce et al. (2020b) and this assumption might not be entirely correct. The strong complexation site put forward by Durce et al. (2020b) to describe their complexation data is apparently absent on DOM_$NaClO_4$ which would, at least partly, explain the lower effect of BC DOM on the Sn(IV) sorption observed here than predicted. Allowing the DOM–Sn(IV) complexation constant to vary (Model 6), the best fit of the sorption data was obtained by considering one complexation site on BC DOM with the complexation constant as reported in Table 5. The optimized value of $log\ K_6$ was 0.6 log unit lower than $log\ K_w^{**(Sn\text{-}DOM)}$. The lower constant, together with the absence of a strong complexation site, would indicate a significantly lower affinity of DOM_$NaClO_4$ towards Sn(IV) than the DOM batch used by Durce et al. (2020b).

On the other hand, the sorption of BC DOM on IdP could also limit its effect on the Sn(IV) sorption. It was however reported by Bruggeman et al. (2010), that BC DOM didn't sorb strongly on Illite and the authors neglected the contribution of DOM sorption on the sorption of Eu(III). However, even if limited, the formation of ternary complexes Sn(IV)-DOM-IdP or DOM-Sn(IV)-IdP would also result in an apparent lower effect of BC DOM complexation on the Sn(IV) sorption. The stoichiometry of the DOM-Sn(IV) complex was not elucidated and the possibly positively charged complexes could also sorb on IdP.
The formation of DOM–Sn(IV)-Clay ternary complexes mediated by Sn(IV) was tested by implementing in the model simple 1:1 reactions with similar constants for the formation of $\equiv S^sOSnDOM_s^{2+}$and $\equiv S^sOSnDOM\_w^{2+}$ (Model 5). The best fit to the experimental data was obtained with the constant value as reported in Table 16. The sorption of Sn(IV) was fully controlled by the sorption of the $SnDOM_w^{3+}$complexes, while the model was insensitive to the formation of $\equiv S^sOSnDOM\_s^{2+}$.

The modelled data described well the experimental points, both by modifying the complexation constant DOM-Sn(IV) and by introducing the formation of ternary complexes DOM-Sn(IV)-Clay. It was, however, rather unexpected that two batches of DOM originating from the same pore water would behave so differently with respect to their affinity for Sn(IV). The difference between the prediction based on the results of Durce et al. (2020b) is therefore assumed to be, at least partly, due to the formation of ternary complexes DOM-Sn(IV)-Clay, though the exact forming mechanisms of these complexes and their stoichiometry remain unknown at this stage.

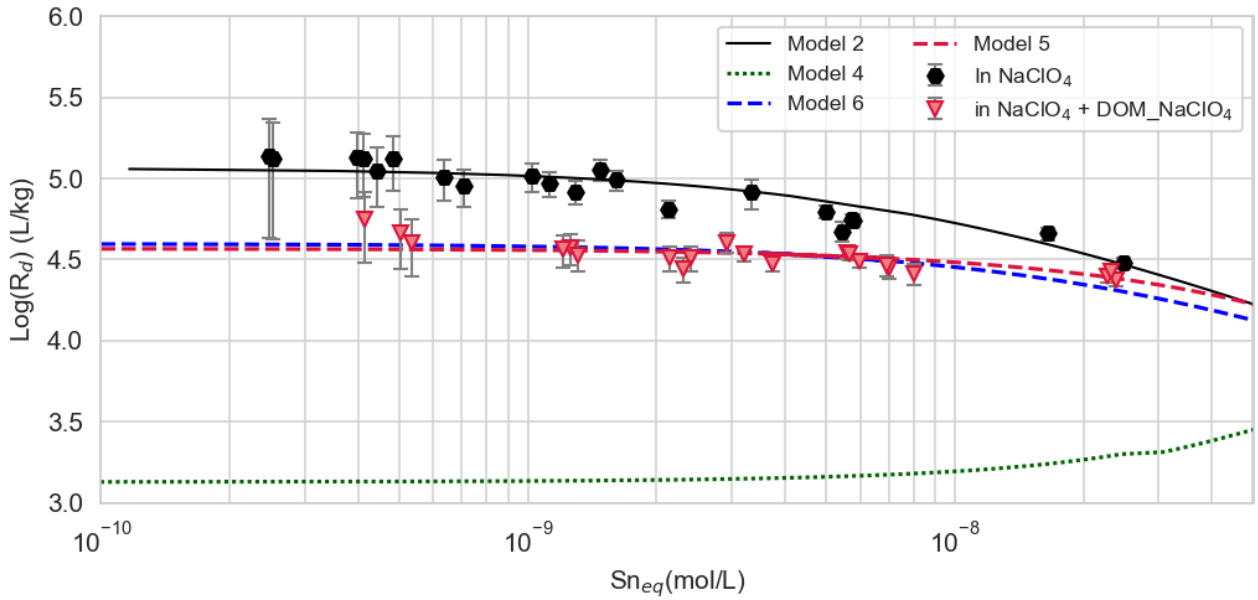

Figure 9. Sn(IV) sorption isotherm on IdP in $NaClO_4$ 0.017 M in presence and absence of 4.5 ± 2.8 ppmC DOM_$NaClO_4$, experimental and modelling results

3.4.2 Sorption isotherm onto STx-1b

The experimental sorption isotherm of Sn(IV) on STx-1b in $NaClO_4$ 0.017 M in presence of DOM_$NaClO_4$ is reported in Figure 10, together with the results obtained in pure $NaClO_4$ 0.017 M.

As observed in other conditions, different solid/liquid ratios lead to different results. The same range of Sn(IV) concentrations was used for the two solid-liquid ratios and the decrease of $log\ R_d$ with the increase of solid/liquid ratio is clearly visible on Figure 10. However, with an average $log\ R_d$ of 4.31 ± 0.10 and 4.00 ± 0.20 for S/L of 0.11 and 0.56 g/L, respectively, the solid/liquid ratio effect appears less pronounced than observed for the experiment in absence of DOM. In agreement with

the results obtained on IdP, the presence of BC DOM reduces the Sn(IV) sorption on STx-1b, in all the conditions (S/L, Sn(IV) concentration), in comparison to the pure $NaClO_4$ system.
The value of $log\ K_6$ determined in the IdP system would translate to the complexation of 70 % of the aqueous Sn(IV) at pH 8.43 and for a DOM_$NaClO_4$ concentration of 11.9 ppmC. This would reduce the R_d values with the same proportion in comparison to the $NaClO_4$ system. The resulting average $log\ K_d$ values for each solid-ratio are reported in blue and green in Figure 10. As it can be observed, at the lowest solid/liquid ratio, it matches relatively well the experimental data though it slightly underestimates the effect of Sn(IV)-DOM complexation. However, the opposite trend is observed at a S/L of 0.56 g/L at which the use of $log\ K_6$ as determined for IdP would overestimate the effect of Sn(IV)-DOM complexation on the sorption. This different behaviour according to the solid/liquid ratio remains unfortunately unclear.

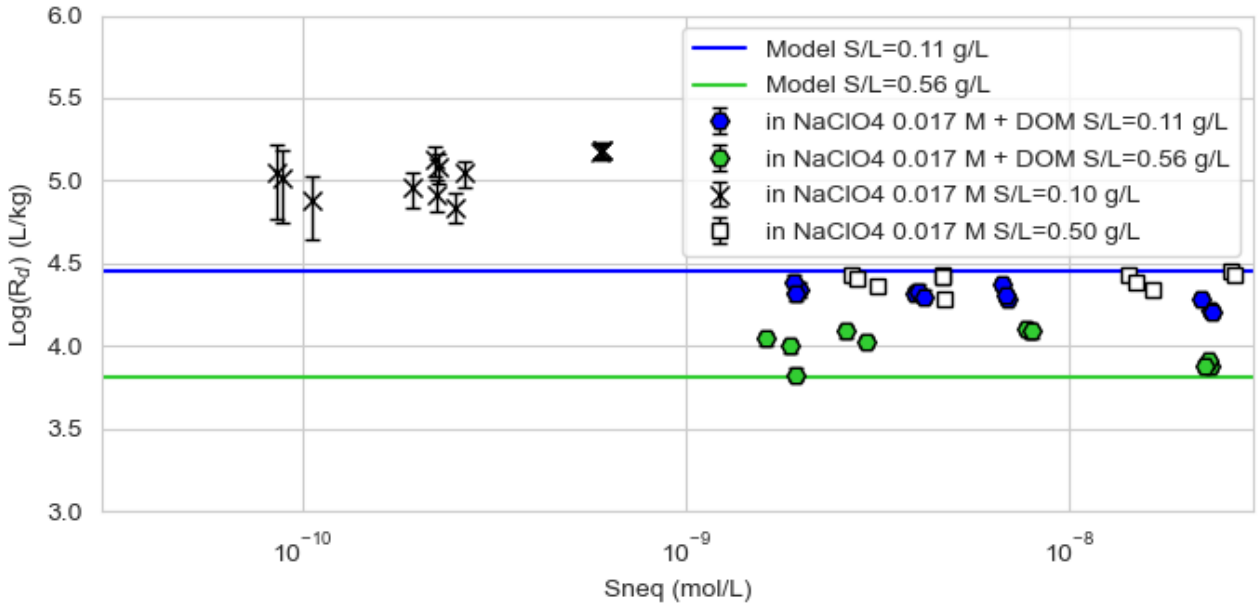

Figure 10. Sn(IV) sorption isotherm on STx-1b in $NaClO_4$ 0.017 M in presence of 11.9 ± 1.2 ppmC DOM_$NaClO_4$ at pH 8.43 ± 0.07. The lines correspond for each S/L to the average $log\ K_{d(DOM)}$ calculated such as $log\ K_{d(DOM)} = log\ (K_{d(NaClO4)} \times (1 - 0.70))$

3.5 Sorption of Sn(IV) onto pure clay minerals in SSW

3.5.1 Sorption isotherm onto IdP

The experimental sorption isotherm of Sn(IV) on IdP in SSW is reported in Figure 11, together with the results obtained in $NaClO_4$ and of the two models, Model 2 and Model 3 adapted to the pH of the experiment and to the carbonate content of SSW.

In comparison to the $NaClO_4$ system, the *log* R_d values calculated in the SSW are slightly lower. The modelling approach including only surface complexation with (Model 3) or without (Model 2) aqueous complexation with the carbonates fails to predict this decrease. Indeed the integration of the complexation with carbonate, as determined in section 3.3.1, does not change the prediction and the results of Model 2 and 3 overlap. None of the tested models takes into account possible competitive sorption between Sn(IV) and the ions present in the SSW. As discussed in section 2.6.2.4, we indeed assumed this competition as negligible with regards to the different chemistry of Sn(IV) with the other ions in presence. Not many literature studies focus on the effect of competitive sorption between major cations/anions and strongly sorbed elements and it is difficult to include it in our model. However, though on a performance assessment point of view the salinity effect here observed probably falls within the error margin, on a phenomenological point of view, investigating more in depth this effect would allow a better comprehension of the mechanisms controlling sorption at high salinity.

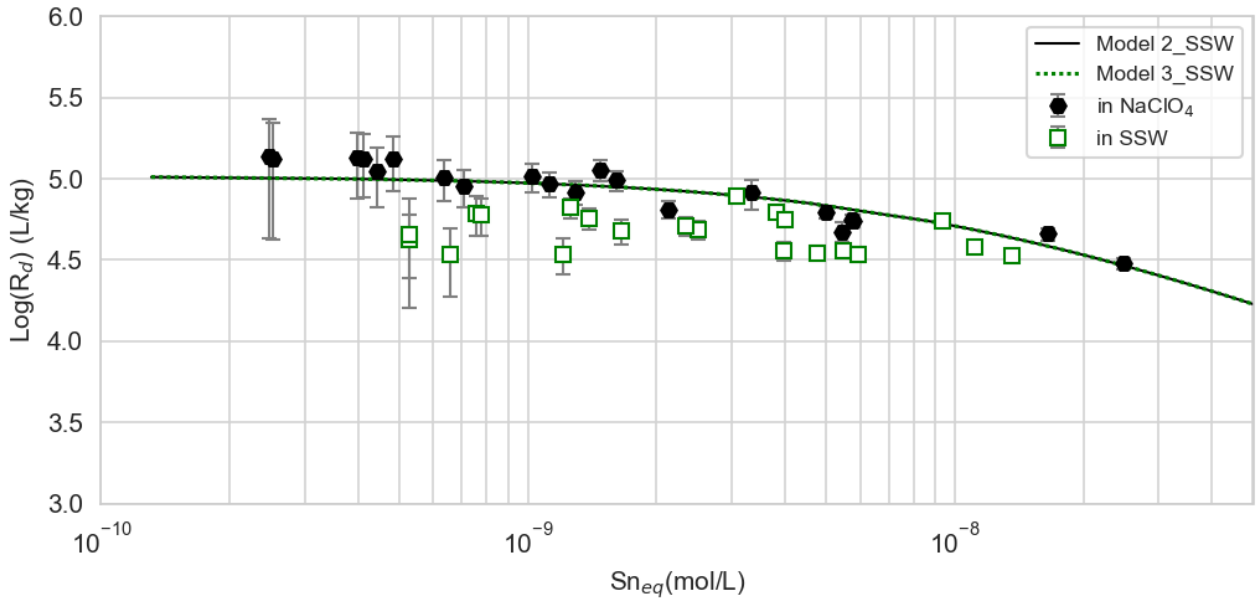

Figure 11. Sn(IV) sorption isotherm on IdP in SSW and in 0.017 M $NaClO_4$, experimental and modelling results

3.5.2 Sorption isotherm onto STx-1b

The experimental sorption isotherm of Sn(IV) on STx-1b in SSW is reported in Figure 12, together with the results obtained in $NaClO_4$ 0.017 M.

Despite a high dispersion of the data obtained at a S/L of 0.52 g/L, it appears that the $log\ R_d$ values of Sn(IV) on STx-1b in SSW do not show an obvious dependence on the experimental solid/liquid ratio on the contrary to all the other investigated conditions. Though this result is not fully understood, it might, as discussed in section 3.2.2, be correlated with the higher salinity of seawater leading to a better efficiency of the centrifugation step. The better cohesion of the STx-1b particles would allow them to better settle, which would annihilate the apparent effect of the solid/liquid ratio on the sorption. This hypothesis remains however to be verified experimentally.

At a solid/liquid ratio of 0.10-0.11 g/L, the increase of salinity between SSW and $NaClO_4$ 0.017 M does not show a strong influence on the sorption of Sn(IV) on STx-1b. A slight increase of the $log\ R_d$ values could be observed, but due to the data dispersion it is difficult to conclude. At a solid/liquid ratio of 0.52-0.50 g/L, a strong difference is observed between SSW and $NaClO_4$ 0.017 M but it is most likely the result of a different effect of the solid/liquid ratio in the two conditions. In SSW, the $log\ R_d$ values are consistent at the two solid/liquid ratios used. The apparent shift of the values obtained at 0.50- 0.52 g/L towards the values obtained at 0.10- 0.11 g/L in comparison to $NaClO_4$ 0.017 M tends to support our previous observation that the sorption results obtained at the lowest solid/liquid ratio are more consistent.

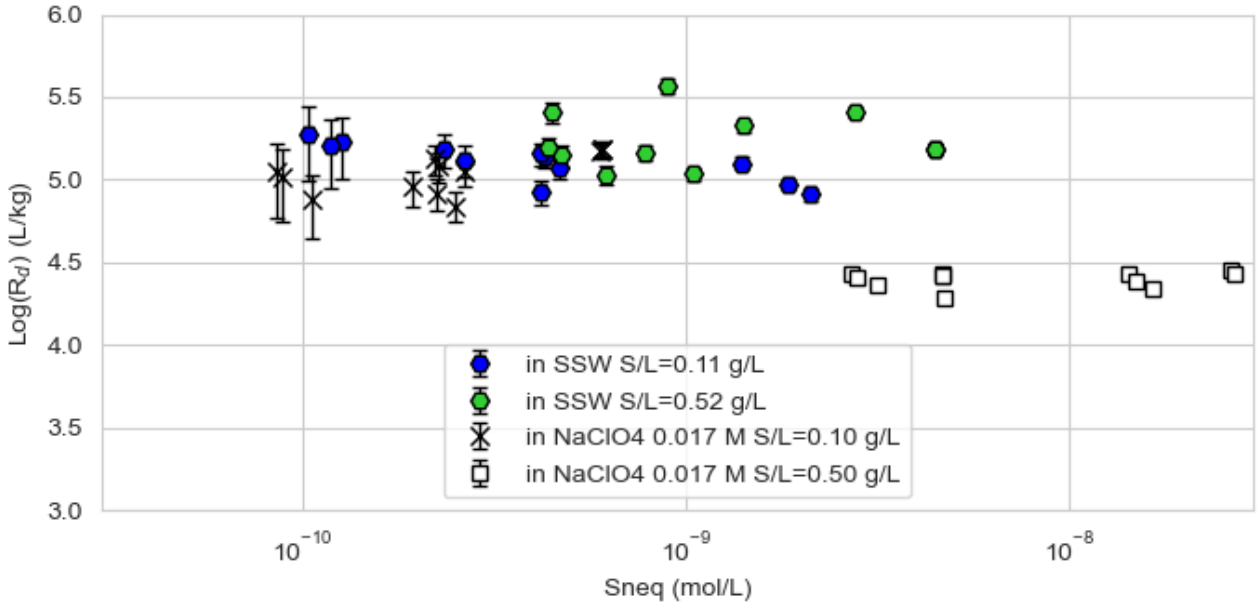

Figure 12. Sn(IV) sorption isotherm on STx-1b in SSW at pH 8.24 ± 0.04.

3.6 Sorption of Sn(IV) on Boom Clay

The experimental sorption isotherm of Sn(IV) on BC in SPRING water is reported in Figure 13, together with the results of the models, Model_CA_1, Model_CA_2, Model_CA_3 and Model_CA_4.

The experimental data are presented either as a function of Sn_{eq}, as calculated from the measured activity (Equation (1)) or recalculated to take into account the concentration of natural Sn, as measured in the blank suspensions. The presence of natural Sn affects only the low concentration points, where it shifts the sorption isotherm towards higher equilibrium Sn concentrations. Except for the obvious outlier, the sorption of Sn(IV) on BC is linear until an equilibrium concentration of ~2×10^{-8} mol/L. Beyond, the $log\ R_d$ values start to gradually decrease, possibly due to a gradual saturation of the strong sorption sites. In comparison with the pure clay systems, the Sn(IV) sorption on BC is lower, which can be expected considering that only 35 wt% of BC is made of 2:1 clay minerals. Yet, as shown by Model_CA_1, the sorption is overestimated when only taking into account the BC 2:1 clay mineral content and the optimized Sn(IV) sorption properties of IdP (Table 16).
Taking into account the Sn(IV)-carbonate complexation with the $log\ k_5$ value determined on IdP (Model_CA_2) improves the fit, but the Sn(IV) uptake is still overestimated in comparison to the experimental results.
The integration in the model of Sn(IV) complexation with DOM contained in the SPRING water using the value of $log\ k_6$ optimized from the IdP experiments (Model_CA_3) predicts a strong reduction of the Sn(IV) sorption, underestimating the experimental data. On the other hand, integrating the formation of DOM-Sn(IV)-ternary complexes as determined on IdP resulted in an overestimation of the Sn(IV) sorption. The shift in predicted $log\ R_d$ values between Model_CA_2, Model_CA_3 and Model_CA_4 highlights the high sensitivity of the model to the complexation of Sn(IV) with DOM.

In present day BC conditions, the speciation of Sn(IV) is mostly controlled by its complexation to DOM and so is its sorption onto clay minerals. Unfortunately, DOM is a complex system on its own and a good description of its aqueous complexation behaviour and sorption properties is difficult to achieve. None of the modelling approaches calibrated on the IdP system, i.e., Sn(IV) surface complexation with DOM-Sn(IV) aqueous complexation with or without sorption of the formed complexes, was able to accurately predict the Sn(IV) sorption on BC.
The interaction of DOM with clay and/or oxides is a complicated process, which often leads to sorptive fractionation and affects the ligand properties of DOM (Reiller, 2012). Due to this complexity and to the resulting uncertainty on the real DOM sorption mechanism and its impact on RNs/Metals sorption onto clays modelling ternary systems clay-DOM-metals/RNs was proven not easy and rarely predictive, especially for elements with a challenging chemistry such as tetravalent metals (Reiller, 2012). In the case of Sn(IV), it appears that the use of a component additivity approach does not lead to a good description of its sorption onto BC. The modelling of the ternary system IdP-BC DOM-Sn(IV) already required an optimization of the DOM-Sn(IV) complexation constant in comparison to the binary system BC DOM-Sn(IV) reported by Durce et al. (2020b). This already pointed out the fragility of the CA approach. As previously discussed (section 2.6.2.5), DOM in SPRING is different than DOM_NaClO4. DOM_NaClO4 contains larger molecules than SPRING DOM, which could display a different reactivity towards Sn(IV) and towards IdP/BC, leading to an apparent lower DOM contribution in the Sn(IV) sorption onto BC Moreover, contrary to the IdP system, BC DOM was in equilibrium with BC and the presence of DOM coated to the BC surface and/or of solid organic matter could affect the extent and the nature of the ternary Sn(IV)-DOM-Clay complexes. The strong complexation of Sn(IV) to DOM in the investigated conditions, the heterogeneity of BC DOM, the uncertainty on the aqueous DOM chemistry and on its sorption to clay fragilize the model here developed, which appears not robust enough to accurately predict Sn(IV) sorption onto BC. A predictive model would require the integration of more knowledge on the DOM behaviour with respect to both its ligand properties and sorption properties. Nevertheless, the use of the CA approach already gives access to a rough estimation of the Sn(IV) sorption with a prediction of the log R_d values which differ only by a maximum of 0.5 log unit from the experimental values.

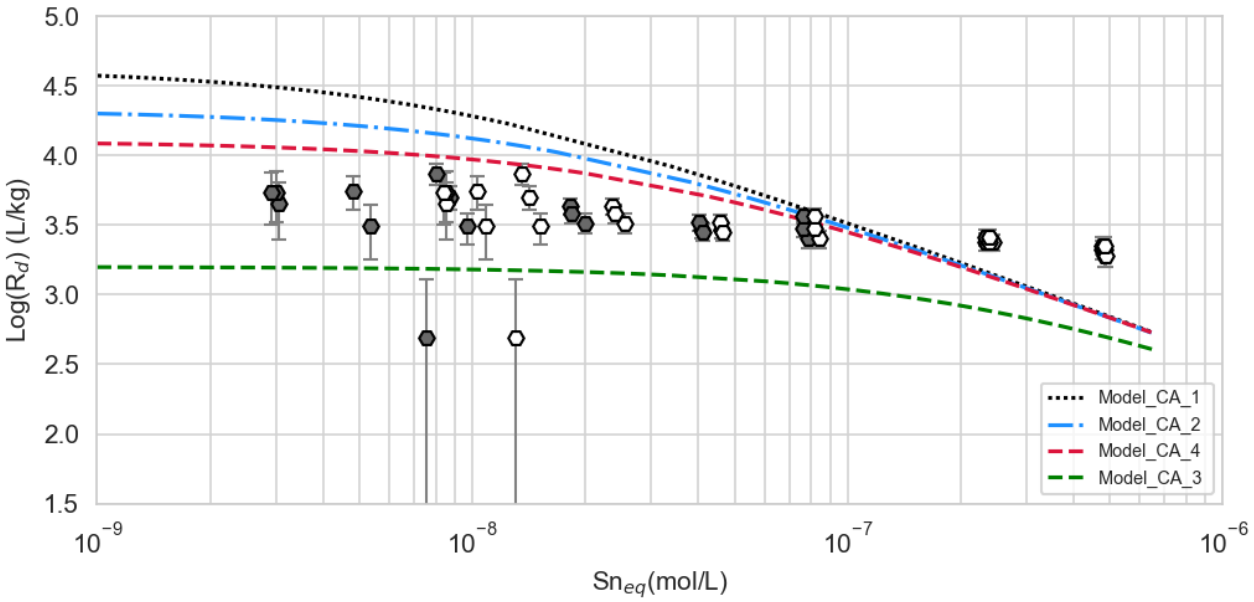

Figure 13. Sn(IV) sorption isotherm on BC in SPRING water at pH 8.41 ± 0.02, experimental and modelling results. Grey markers= experimental data, empty markers= experimental data recalculated taking into account the natural Sn concentration such as Sn_{eq}(recalculated)=Sn_{eq}+$Sn_{natural}$.

4 Conclusions

The various experiments performed to assess the Sn(IV) sorption onto the pure clays Illite du Puy and Montmorillonite STx-1b showed a strong uptake of Sn(IV) with $log\ Rd$ values ranging between 4.2 and 5.6, at pH ~8.4 and in absence of DOM. This is in the same order of magnitude than other tetravalent elements such as Th(IV) (Bradbury and Baeyens, 2017; Marques Fernandes et al., 2015). The presence of DOM was, however, shown to significantly decrease the sorption on the two clays, even at low DOM concentration. On IdP a reduction of ~0.5 log unit was observed in $log\ Rd$ values in presence of 4.5 ppmC. This result is in line with the strong complexation of Sn(IV) with BC DOM reported by Durce et al. (2020b), though it was found to have less influence than predicted by the Sn(IV)-DOM complexation constants reported by Durce et al. (2020b). The difference was attributed to the sorption of the formed Sn(IV)-DOM complexes and/or to the heterogeneity of the used DOM batches. On the other hand, the presence of carbonate was shown to have a minor effect in 0.015 M of $NaHCO_3$ with a $log\ R_d$ decrease on IdP lower than 0.3 log unit in comparison to the 0.017 M $NaClO_4$ system.
The effect of salinity is less clear and showed to be opposite on the two clays. It slightly decreased sorption on IdP with an average drop in $log\ R_d$ values of 0.2 ± 0.11 log unit in comparison with the $NaClO_4$ 0.017 system and on the investigated range of concentrations. Though the effect was minor (average change of 0.07 log unit for the $log\ R_d$ values at S/L of 0.1 g/L) it appeared to increase on STx-1b. The modification of the uptake in SSW conditions could not be reproduced by only considering the contribution of the carbonates contained in SSW and hence could indicate the presence of other phenomena not taken here into account such as electrostatic effects or competitive sorption.

Overall, the results showed good consistency between the two clays, though some uncertainty persists on the results obtained onto STx-1b due to the influence of the experimental solid/liquid ratio. Some more in-depth investigations should be dedicated to this issue to understand its source and to avoid it in future studies on the STx-1b montmorillonite.
The sorption of Sn(IV) was found consistently lower on both clays than previously reported by Bradbury and Baeyens (2005b) and Bradbury and Baeyens (2009). The reason for this difference was not elucidated, but could be due to the use of different batches of clays or to different experimental conditions or protocols such as different phase separation conditions. Nevertheless, the results obtained here in the different experiments are consistent between them and they are conservative with respect to the retardation of Sn(IV) and as such can be used for safety assessment.

The modelling approach combining the 2SPNE SC model with Sn(IV) aqueous complexation with BC DOM and carbonate was able, with an optimization of the constants, to well describe most of the obtained sorption datasets on Illite du Puy. Only the Sn(IV) sorption behaviour in SSW could not be accurately depicted, highlighting possible further refinement of the Sn(IV) sorption model to account for competitive sorption and/or electrostatics.
The component additivity approach built on the results obtained on IdP provided a rough estimation of the Sn(IV) sorption onto BC under present day BC conditions, but it failed in accurately predicting it. The deviation between prediction and experimental results was attributed to the high sensitivity of the model to the Sn(IV)-DOM complexation and to a lack of mechanistic understanding on the DOM behaviour with respect to both its ligand properties and sorption properties to properly estimate the role of DOM onto Sn(IV) sorption. This highlighted the need for more in-depth understanding and testing/developing of mechanistic models on DOM behaviour in the binary systems DOM-RNs and Clay-DOM to further being able to predict the ternary systems Clay-DOM-RNs.

In addition to gaining new insight on the Sn(IV) sorption on pure clay minerals and BC, this study also aimed at being a test case for a future sorption experimental program. On the one hand, the followed methodology led to a robust set of experimental data for IdP. Besides some difficulties, valid at least for Sn(IV), in extending the data obtained at low ionic strength to higher saline conditions, the thermodynamic sorption model (TSM) was able to satisfactorily depict the Sn(IV) sorption on IdP in conditions relevant for a scenario of a nuclear waste repository in BC. On the other hand, the inconsistency in the experimental results obtained on STx-1b montmorillonite at different solid/liquid ratios reaffirmed the need for a rigorous preliminary sorption study which should include, a minima, the investigation of the sorption kinetics, of the effect of solid/liquid ratio and of the effect of solid/liquid phase separation method. The failure of the component additivity approach in predicting the sorption of Sn(IV) onto BC highlighted the need for a more mechanistic understanding and modelling of the role of OM on RN sorption on clay. This is especially needed in an OM-rich environment such as Boom Clay to predict the sorption of RNs in the 'NOM-related transport' group as defined in the grouping approach detailed by Bruggeman and Maes (2017). One should also keep in mind that he lack of thermodynamic data available on Sn(IV) speciation and the lack of agreement between databases render all the modelling exercises and the resulting TSM highly conditional. The possibility to remodel the experimental datasets when more thermodynamic data will be made available and validated, should definitely be left open.

5 References

Altmann, S., Aertsens, M., Appelo, T., Bruggeman, C., Gaboreau, S., Glaus, M., Jacquier, P., Kupcik, T., Maes, N., Montoya, V., Rabung, T., Robinet, J.-C., savoye, S., Schaefer, T., Tournassat, C., Van Laer, L. and Van Loon, L. (2015) Processes of Cation Migration in Clayrocks: Final Scientific Report of the Catclay Europeanproject CEA.

Baes, C.F. and Mesmer, R.S. (1977) The Hydrolysis of Cations. John Wiley & Sons, New York. 81, 245-246.

Baeyens, B. and Bradbury, M.H. (1997) A Mechanistic Description of Ni and Zn Sorption on Na-Montmorillonite Part I: Titration and Sorption Measurements. Journal of Contaminant Hydrology 27, 199-222.

Begg, J.D., Edelman, C., Zavarin, M. and Kersting, A.B. (2018) Sorption Kinetics of Plutonium (V)/(Vi) to Three Montmorillonite Clays. Applied Geochemistry 96, 131-137.

Bradbury, M.H. and Baeyens, B. (1997) A Mechanistic Description of Ni and Zn Sorption on Na-Montmorillonite Part Ii: Modelling. Journal of Contaminant Hydrology 27, 223-248.

Bradbury, M.H. and Baeyens, B. (2005a) Experimental Measurements and Modeling of Sorption Competition on Montmorillonite. Geochimica et Cosmochimica Acta 69, 4187-4197.

Bradbury, M.H. and Baeyens, B. (2005b) Modelling the Sorption of Mn(Ii), Co(Ii), Ni(Ii), Zn(Ii), Cd(Ii), Eu(Iii), Am(Iii), Sn(Iv), Th(Iv), Np(V) and U(Vi) on Montmorillonite: Linear Free Energy Relationships and Estimates of Surface Binding Constants for Some Selected Heavy Metals and Actinides. Geochimica et Cosmochimica Acta 69, 875-892.

Bradbury, M.H. and Baeyens, B. (2009) Sorption Modelling on Illite Part I: Titration Measurements and the Sorption of Ni, Co, Eu and Sn. Geochimica et Cosmochimica Acta 73, 990-1003.

Bradbury, M.H. and Baeyens, B. (2017) The Development of a Thermodynamic Sorption Data Base for Montmorillonite and the Application to Bentonite, Switzerland, p. 105.

Brown, P., Curti, E. and Grambow, B. (2008) Chemical Thermodynamics 8. Chemical Thermodynamics of Zirconium. Eds., OECD Publications, Paris, France. .

Bruggeman, C., Liu, D.J. and Maes, N. (2010) Influence of Boom Clay Organic Matter on the Adsorption of $Eu^{(3+)}$ by Illite - Geochemical Modelling Using the Component Additivity Approach. Radiochimica Acta 98, 597-605.

Bruggeman, C. and Maes, N. (2017) Radionuclide Migration and Retention in Boom Clay, External report SCK•CEN-, Mol, Belgium.

Castellini, E., Malferrari, D., Bernini, F., Brigatti, M.F., Castro, G.R., Medici, L., Mucci, A. and Borsari, M. (2017) Baseline Studies of the Clay Minerals Society Source Clay Montmorillonite Stx-1b. Clays and Clay Minerals 65, 220-233.

Dähn, R., Baeyens, B. and Fernandes, M.M. (2021) Zn Uptake by Illite and Argillaceous Rocks. Geochimica et Cosmochimica Acta 312, 180-193.

Davies, C.W. (1962) Ion Association. Butterworths, London.

De Craen, M., Wang, L., Van Geet, M. and Moors, H. (2004) Geochemistry of Boom Clay Pore Water at the Mol Site, Scientific report. SCK•CEN, Mol, Belgium.

Durce, D., Bruggeman, C., Maes, N., Van Ravestyn, L. and Brabants, G. (2015) Partitioning of Organic Matter in Boom Clay: Leachable Vs Mobile Organic Matter. Applied Geochemistry 63, 169-181.

Durce, D., Salah, S., Van Laer, L., Wang, L., Maes, N. and Brassinnes, S. (2022) Sn(Iv) Sorption onto Illite and Boom Clay: Effect of Carbonate and Dissolved Organic Matter, Minerals.

Durce, D., Salah, S. and Wang, L. (2020a) Interaction of Zirconium and Tin with Boom Clay Dissolved Organic Matter. External report SCK•CEN-ER-0556 (Mol, Belgium).

Durce, D., Salah, S., Wang, L. and Maes, N. (2020b) Complexation of Sn with Boom Clay Natural Organic Matter under Nuclear Waste Repository Conditions. Applied Geochemistry 123, 104775.

Fernandes, M.M., Baeyens, B., Marques Fernandes, M. and Baeyens, B. (2019) Cation Exchange and Surface Complexation of Lead on Montmorillonite and Illite Including Competitive Adsorption Effects. Applied Geochemistry 100, 190-202.

Gamsjäger, H., Gajda, T., Sangster, J., Saxena, S.K. and Voigt, W. (2012) Chemical Thermodynamics 12. Chemical Thermodynamics of Tin. Eds., OECD Publications. , Paris, France.

Grivé, M., Duro, L., Colàs, E. and Giffaut, E. (2015) Thermodynamic Data Selection Applied to Radionuclides and Chemotoxic Elements: An Overview of the Thermochimie-Tdb. Applied Geochemistry 55, 85-94.

Hummel, W., Berner, U., Curti, E., Pearson, F. and Thoenen, T. (2002) Nagra/Psi Chemical Thermodynamic Data Base 01/0. Nagra/Psi Chemical Thermodynamic Data Base 01/01. Nagra. Ntb 02-06. Pp. 564. Http://Www.Nagra.Ch/Data/Documents/Database/Dokumente/$Default/Default%20folder/Publikationen/Ntbs%202001-2010/E_Ntb02-16.Pdf. Nagra Technical Report NTB 02-16, Nagra, Wettingen, Switzerland; and Universal Publishers/uPublish.com, Parkland, Florida, ISBN 1-58112-620-4.

Kester, D.R., Duedall, I.W., Connors, D.N. and Pytkowicz, R.M. (1967) Preparation of Artificial Seawater1. 12, 176-179.

Marques Fernandes, M., Vér, N. and Baeyens, B. (2015) Predicting the Uptake of Cs, Co, Ni, Eu, Th and U on Argillaceous Rocks Using Sorption Models for Illite. Applied Geochemistry 59, 189-199.

Parkhurst, D.L. and Appelo, C. (2013) Description of Input and Examples for Phreeqc Version 3—a Computer Program for Speciation, Batch-Reaction, One-Dimensional Transport, and Inverse Geochemical Calculations. US geological survey techniques and methods 6, 497.

Payne, T., Brendler, V., Ochs, M., Baeyens, B., Brown, P.L., Davis, J., Ekberg, C., Kulik, D., Lützenkirchen, J., Missana, T., Tachi, Y., Van Loon, L. and Altmann, S. (2013) Guidelines for Thermodynamic Sorption Modelling in the Context of Radioactive Waste Disposal. Environmental Modelling & Software 42, 143-156.

Poeter, E.P., Hill, M.C., Lu, D., Tiedeman, C. and Mehl, S.W. (2014) Ucode_2014, with New Capabilities to Define Parameters Unique to Predictions, Calculate Weights Using Simulated Values, Estimate Parameters with Svd, Evaluate Uncertainty with Mcmc, and More.

Rabung, T., Pierret, M.C., Bauer, A., Geckeis, H., Bradbury, M.H. and Baeyens, B. (2005) Sorption of Eu(Iii)/Cm(Iii) on Ca-Montmorillonite and Na-Illite. Part 1: Batch Sorption and Time-Resolved Laser Fluorescence Spectroscopy Experiments. Geochimica et Cosmochimica Acta 69, 5393-5402.

Reiller, P.E. (2012) Modelling Metal–Humic Substances–Surface Systems: Reasons for Success, Failure and Possible Routes for Peace of Mind. Mineralogical Magazine 76, 2643-2658.

Salah, S. and Wang, L. (2017) Speciation and Solubility Calculations for Waste Relevant Radionuclides in Boom Clay, External report SCK•CEN, Mol, Belgium.

Salah, S. and Wang, L. (2018) Speciation and Solubility in Essen Porewater and Seawater Compositions. Technical report SCK•CEN-T-0127 (Mol, Belgium).

Semenkova, A.S., Evsiunina, M.V., Verma, P.K., Mohapatra, P.K., Petrov, V.G., Seregina, I.F., Bolshov, M.A., Krupskaya, V.V., Romanchuk, A.Y. and Kalmykov, S.N. (2018) Cs+ Sorption onto Kutch Clays: Influence of Competing Ions. Applied Clay Science 166, 88-93.

Soltermann, D., Marques Fernandes, M., Baeyens, B., Dähn, R., Joshi, P.A., Scheinost, A.C. and Gorski, C.A. (2014a) Fe(Ii) Uptake on Natural Montmorillonites. I. Macroscopic and Spectroscopic Characterization. Environmental Science & Technology 48, 8688-8697.

Soltermann, D., Marques Fernandes, M., Baeyens, B., Miehé-Brendlé, J. and Dähn, R. (2014b) Competitive Fe(Ii)–Zn(Ii) Uptake on a Synthetic Montmorillonite. Environmental Science & Technology 48, 190-198.

Sugiura, Y., Ishidera, T. and Tachi, Y. (2021) Surface Complexation of Ca and Competitive Sorption of Divalent Cations on Montmorillonite under Alkaline Conditions. Applied Clay Science 200, 105910.

Tertre, E., Berger, G., Castet, S., Loubet, M. and Giffaut, E. (2005) Experimental Sorption of Ni2+, Cs+ and Ln3+ onto a Montmorillonite up to 150°C. Geochimica et Cosmochimica Acta 69, 4937-4948.

Thomas, P. (2018) Determination of Tic and Toc in Boom Clay Pore Waters - Validation and Measurement Uncertainty. Technical report SCK•CEN-T-0143 (Mol, Belgium).

Thomas, P. and Durce, D. (2022a) Protocol for the Acid-Base Titration of Illite Du Puy and
Montmorillonite Stx-1b. Technical report SCK•CEN-T-0714 (Mol, Belgium).

Thomas, P. and Durce, D. (2022b) Results of the Acid-Base Titrations of Illite Du Puy and Montmorillonite
Stx-1b. Technical report SCK•CEN-T-0743 (Mol, Belgium).

Van Laer, L. (2018) Guidelines for Batch Suspension Experiments under Saline Conditions. Technical Report T-0113. SCK-CEN, Belgium.

Van Laer, L. (2019) Guidelines for Batch Suspension Experiments under Saline Conditions. Studiecentrum voor Kernenergie.

Van Laer, L., Aertsens, M., Verhaegen, D. and Van Gompel, M. (2020) Impact of Saline Conditions on the Transport of Hto and Iodine in Boom Clay. External scientific Report ER-0548. SCK-CEN, Belgium.

Van Laer, L., Durce, D., Salah, S. and N., M. (2016) Sorption Studies on Boom Clay and Clay Minerals – Status 2016. External scientific Report ER-0346. SCK-CEN, Belgium.

W.Oscarson, D. and B.Hume, H. (1998) Chapter 12 - Effect of the Solid: Liquid Ratio on the Sorption of Sr2+ and Cs+ on Bentonite. Adsorption of Metals by Geomedia
Adsorption of Metals by Geomedia Variables, Mechanisms, and Model Applications, 277-289.

Yang, S., Ren, X., Zhao, G., Shi, W., Montavon, G., Grambow, B. and Wang, X. (2015) Retracted: Competitive Sorption and Selective Sequence of Cu(Ii) and Ni(Ii) on Montmorillonite: Batch, Modeling, Epr and Xas Studies. Geochimica et Cosmochimica Acta 166, 129-145.

6 Experimental data


Edge_experiments.xlsm


Result_isotherm_BC.xlsm


Stx-1b_isotherms.xlsm


IdP_isotherms.xlsm

A Purification procedure of the STx1-b montmorillonite

This protocol is based on various protocols reported in the literature. Some authors use their montmorillonite sample 'as such', ie without any purification step (Yang et al., 2015). The authors just report the specific surface area (measured with the N_2-BET method) and the CEC of the used clay sample. Some authors focus only on the conditioning of their batch (Rabung et al., 2005) while others add a purification step to remove the carbonates, hydroxyl-aluminium compounds and soluble salts by acidification (Baeyens and Bradbury, 1997; Begg et al., 2018; Tertre et al., 2005) or even the iron oxides with citrate buffer (Semenkova et al., 2018). The size fractionation of the montmorillonite varies also from groups to groups. Some groups work with the so called clay fraction, i.e < 2 µm (Begg et al., 2018; Rabung et al., 2005), others with larger fractions (< 75 µm, (Semenkova et al., 2018)) and others with very fine clay particles (< 0.5 µm, (Baeyens and Bradbury, 1997)).

It is clear that the degree of purification/conditioning and fractionation depend on the focus of the study. Raw materials can be used for a crude Kd determination but if the objective is the determination of surface complexation constants and/or selectivity coefficients a more in depth purification/conditioning procedure is required as the presence of impurities could impact both the sorption and the speciation of the elements of interest. The use of finer fractions allows to work with the pure clay material while coarser samples could contains some other minerals such as quartz.

With respect to the objectives of this study, the established protocol is the following:

Removal of carbonates, hydroxyl-aluminium compounds and soluble salts

- 20 g of the raw clay material is suspended in 200 mL 0.001 M HCl in a Nalgene centrifuge bottle.
- The suspension is shaken for 30 min, let to settle and the pH is measured
- The pH is adjusted to pH 3 by addition of 1 M HCl. Pay attention not to go below pH 3 (dissolution of the clay)
- The suspension is shaken for another 15 min, let to settle and the pH adjust to 3 if necessary
- The suspension is then shaken for 1h
- The suspension is then directly centrifuged 30 min at 20 000 x g (cut off 75 nm)
- The supernatant is discarded

!! at pH 3 the clay starts to dissolve and the contact time with the acid solution should be limited. The time span of the described should be respected.

Conversion to Na-form

- The solid is resuspended in 80 mL of 1 M NaCl. Because of aggregation the resuspension is difficult. Make use of a spatula to try to break as much as possible the aggregate, you can also make use of the vortex.
- The suspension is shaken for 3 h and centrifuged 30 min at 21 000 x g
- The supernatant is discarded and the procedure is repeated 2 more times
- The pH of the supernatant after the last centrifugation is checked

After this step, the clay has become a very 'solid mass' / 'a big aggregate'

Rinsing the clay

Cleaning of the dialysis membranes

The dialysis membranes used are conditioned in a sodium azide solution and should never be allowed to dry out. One segments of ~25 cm is cut. The roll is then put back into its sodium azide solution and in the fridge. The membrane segments are soaked in UP water and the water is renewed each 30 min for a total of at least 3 renewals. The segments are then thoroughly rinsed with UP water (inside and outside) and stored in UP water until use.

Rinsing the clay suspension

- 100 mL of UP water or 0.01 M $NaClO_4$ (depending on the study) are added to the pot containing the wet clay. The clay is reput in suspension with the use of a spatula or a vortex.
- The dialysis membrane segments (one per pot) are closed on one side using the dedicated closures (check in lab 37).
- The clay suspension is transferred in one segment and the other side of the membrane is closed with the dedicated closure.
- The dialysis bag is then immersed in 2 L of UP water or 0.01 M $NaClO_4$ (depending on the study) and the system is mechanically shaken.
- After 1 day, the conductivity of the outside solution is measured and if still higher than the conductivity of UP water or 0.01 M $NaClO_4$ (depending on the study), the solution is discarded and replaced by fresh solution.
- The procedure is repeated until the conductivity of the outside solution is lower than the conductivity of UP water or 0.01 M $NaClO_4$ (depending on the study) (~ 7 to 10 days)

Fractionation of the clay (75 nm< Ø <2 µm)

- The clay is transferred from the dialysis bag to a centrifuge bottle
- 50 mL of UP water or 0.01 M $NaClO_4$ (depending on the study) are added and the bottle is put on the shaker for 1 hour
- The suspension is centrifuged for 30 min at 20000*g and the supernatant discarded
- 100 mL of UP water or 0.01 M $NaClO_4$ (depending on the study) are added and the suspension is put on a shaker for 3 h
- The suspension is centrifuged at 1000 rpm for 5 min and 27s
- The supernatant is collected and transferred to another centrifuge bottle
- 100 mL of UP water or 0.01 M $NaClO_4$ (depending on the study) are added to the solid and the procedure is repeated
- The procedure is repeated until the supernatant is clear (no particles in suspension visible)
- The collected supernatants are centrifuged 30 min at 21 000 x g, the supernatants are discarded and the solids collected

Further use

For the purpose of the experiments, a fraction of the purified montmorillonite is left in suspension in 0.01 M $NaClO_4$ at a solid/liquid ratio of 147 g/L. The other fraction is freeze-dried.

B Procedure for Synthetic Seawater preparation

The nature and amount of the salts used for the preparation are summarized in Table A.1 and Table A.2.

Table A.1. Nature and amount of gravimetric salts used for preparation of 1 L of synthetic seawater.

Gravimetric Salts	Mass (g) to add for 1 L of synthetic seawater
NaCl	23.926
Na_2SO_4	4.008
KCl	0.677
$NaHCO_3$	0.196
KBr	0.098

Table A.2. Nature and amount of volumetric salts used for preparation of 1 L of synthetic seawater.

Volumetric salts	Concentration stock solution (M)	Volume (mL) stock solution to add for 1 L of synthetic seawater
$MgCl_2$, $6H_2O$	1	53.27
$CaCl_2$, $2H_2O$	1	10.33
$SrCl_2$, $6H_2O$	0.1	0.90

All the used salts are reagent grade to limit the presence of impurities that could affect the final composition of the synthetic seawater. To ensure a reliable/constant composition of the solution, the following procedure adapted from Kester et al. (1967) will be followed for the preparation of 1 L of synthetic seawater:

NaCl, Na_2SO_4, KCl, KBr are dried and weighed in anhydrous form. $NaHCO_3$ is weighed without drying due to uncertainty in the composition of the dried forms. The gravimetric salts are mixed with UltraPure (UP) water in a 1 L volumetric flask up to a volume of ~900 mL.

Reagent grade salts of $MgCl_2$, $CaCl_2$ and $SrCl_2$ contain water of hydration which makes direct weighing unsatisfactory and these salts are added volumetrically from concentrated solutions. Stock solutions of 1 M $MgCl_2$,$6H_2O$ and $CaCl_2$,$2H_2O$ and 0.1 M $SrCl_2$,$6H_2O$ are prepared and filtered to remove potential insoluble material (0.22 µm).

According to the concentration of the stock solutions, the right volumes of volumetric salt solutions (cf Table) are added to the solution of gravimetric salts in the volumetric flask and UltraPure water is added to complete up to 1 L. Each addition is weighed.

The synthetic seawater is then filtered at 0.45 µm and introduced to a Ar/0.4% CO_2 glovebox where it is allowed to equilibrate to the atmosphere. At equilibrium, the pH is measured

C Cationic composition of the background solutions, clay suspensions and blank clay suspensions

Table C.1. Cationic composition of $NaHCO_3$ 0.02 M, SSW and $NaClO_4$ 0.023 M. *KCl was added to the solutions to limit clay disturbance Q.L= quantification limit. n.m= not measured. When not mentioned measurements errors are estimated to to 2σ[conc/[conc]= 0.1

Concentrations in mol/L	$NaHCO_3$ 0.02 M*	SSW	$NaClO_4$ 0.023M*	SPRING
Na	1.87E-02	4.51E-01	2.15E-02	1.56E-02 ± 1.3E-03
Mg	1.89E-06	5.22E-02	1.11E-07	9.13E-05 ± 5.8E-06
Al (NoGas)	1.16E-06	5.21E-07	3.54E-08	
Al (He)	1.19E-06	5.49E-07	4.54E-08	4.1E-07 ± 1.4E-07
Si	1.37E-04	1.18E-05	1.62E-05	1.47E-04 ± 4.3E-06
P	1.55E-04	< Q.L	1.13E-04	n.m
S	4.10E-06	2.87E-02	1.69E-05	SO42-: < Q.L S2O32-: < Q.L
K	1.38E-04	9.69E-03	1.55E-04	2.56E-04 ± 2.1E-05
Ca	3.98E-06	1.09E-02	5.39E-07	6.59E-05 ± 2.5E-06
Fe	1.33E-07	1.09E-07	4.48E-08	9.5E-06 ± 2.5E-06
Sr	4.41E-08	1.49E-04	1.98E-08	8.1E-06 ± 4.1E-07
Sn	< Q.L	< Q.L	< Q.L	n.m

Table C.2. Cationic composition of the clay suspensions. n.m= not measured. D.L= detection limit. When not mentioned measurements errors are estimated to to 2σ[conc/[conc]= 0.1 and 0.2 for Sn in IdP_0

Concentrations in mol/L	IdP_0	IdP_1	STx1b_0a	BC_1
Na	n.m	n.m	n.m	n.m
Mg	3.15E-05	1.85E-05	4.87E-05	1.26E-05
Al (NoGas)	2.81E-05	3.44E-05	1.80E-05	3.90E-06
Al (He)	2.86E-05	3.55E-05	1.73E-05	4.34E-06
Si	3.48E-04	8.90E-04	7.82E-04	6.84E-04
P	1.12E-01	8.30E-02	1.22E-02	2.40E-05
K	6.29E-05	1.54E-04	3.00E-05	2.88E-04
Ca	3.76E-05	2.53E-05	3.19E-05	2.94E-04
Ti	3.12E-07	1.56E-07	1.73E-07	1.33E-06
Fe	1.13E-06	6.96E-07	2.07E-06	7.54E-06
Cu	8.67E-06	1.55E-07	4.96E-05	4.16E-07
Zn	4.94E-05	4.30E-07	2.69E-05	1.33E-06
Sn	6.01E-09	< D.L	< D.L	2.05E-08

Table C.2. Anionic composition of the clay suspensions. When not mentioned measurements errors are estimated to to 2σ[conc/[conc]= 0.1

Concentrations in mol/L	IdP_0	IdP_1	Stx1b_0a
Cl^-	1.71E-04	1.76E-04	3.39E-04
NO_3^-	1.11E-04	8.34E-05	1.04E-04
SO_4^{2-}	9.31E-06	5.75E-06	1.32E-05
PO_4^{3-}	9.21E-05	6.98E-05	1.01E-05

Table C.3. Cationic composition of the STx-1b suspensions obtained at different solid/liquid ratios. The concentrations were measured after 7 days of contact and centrifugation 2h/20000*g. When not mentioned measurements errors are estimated to to 2σ[conc/[conc]= 0.1

Concentrations in mol/L	S/L= 1.24 g/L	S/L= 0.88 g/L	S/L= 0.60 g/L	S/L= 0.30 g/L	S/L= 0.10 g/L
Mg	1.72E-05	1.56E-05	1.67E-05	2.50E-05	5.82E-06
Al [No G]	1.97E-05	1.90E-05	1.19E-05	6.98E-06	3.08E-03
Al [He]	2.07E-05	2.00E-05	1.26E-05	7.30E-06	3.33E-06
Si	3.33E-04	2.81E-04	1.98E-04	9.79E-05	5.06E-08
K	2.23E-05	2.80E-05	2.68E-05	2.91E-05	2.39E-05
Ca	1.58E-04	1.56E-04	1.97E-04	3.16E-04	1.28E-04
Ti	3.01E-07	2.04E-07	1.75E-07	1.03E-07	6.03E-05
Cr	1.14E-08	1.81E-08	1.86E-08	5.26E-08	3.99E-08
Mn	9.33E-07	9.56E-07	2.30E-06	1.59E-06	1.72E-06
Fe	1.82E-06	1.66E-06	1.35E-06	1.77E-06	4.83E-07
Co	1.31E-09	1.39E-09	2.11E-09	2.28E-09	1.95E-09
Ni	3.56E-07	2.71E-06	5.66E-07	7.14E-07	3.43E-07
Cu	1.09E-06	1.62E-06	1.43E-06	2.34E-06	9.87E-07
Zn	2.45E-06	4.86E-06	3.18E-06	6.62E-06	2.45E-06
Ga	1.38E-08	1.44E-08	1.46E-08	1.08E-08	1.44E-08
As	1.97E-08	1.98E-08	1.52E-08	1.11E-08	9.24E-09
Sr	3.28E-07	3.08E-07	3.68E-07	5.66E-07	2.13E-07
Zr (NoGas)	7.49E-08	5.15E-08	4.23E-08	2.71E-08	3.72E-08
Sn	1.48E-09	8.41E-10	8.00E-10	1.28E-09	1.18E-09
Pb	8.76E-09	1.21E-08	1.12E-08	1.46E-08	1.12E-08

D Data input for 2SPNE/SC-CE model implementation

The clay surface site capacity, protolysis reactions and constants, the cation exchange reactions on planar sites and the corresponding selectivity coefficients and the Sn(IV) hydrolysis constants used as reference in the implementation of the 2SPNE/SC-CE model are reported in the following tables for both Illite du Puy and Montmorillonite Na-SWy-1. The data reported for Montmorillonite Na-SWy-1 are assumed valid for the Stx-1b used in the present work.

Table B.1. Surface site capacities and protolysis constants reported for Illite du Puy by (1) Bradbury and Baeyens (2009) and for Montmorillonite SWy-1 by (2) Bradbury and Baeyens (1997)

	Ilite du Puy[1]	Montmorillonite Na-SWy-1[2]
$\equiv S^{w1}OH + H^+ \leftrightarrow \equiv S^{w1}OH^{2+}$	*log K*= 4.0	*log K*= 4.5
$\equiv S^{w2}OH + H^+ \leftrightarrow \equiv S^{w2}OH^{2+}$	*log K* = 8.5	*log K* = 6.0
$\equiv S^{s}OH + H^+ \leftrightarrow \equiv S^{s}OH^{2+}$	*log K* = 4.0	*log K* = 4.5
$\equiv S^{w1}OH \leftrightarrow \equiv S^{w1}O^- + H^+$	*log K* = -6.2	*log K* = -7.9
$\equiv S^{w2}OH \leftrightarrow \equiv S^{w2}O^- + H^+$	*log K* = -10.5	*log K* = -10.5
$\equiv S^{s}OH \leftrightarrow \equiv S^{s}O^- + H^+$	*log K* = -6.2	*log K* = -7.9
$\equiv S^{w1}OH$	*Capacity= 4× 10-2 mol/kg*	*Capacity= 4× 10-2 mol/kg*
$\equiv S^{w2}OH$	*Capacity= 4× 10-2 mol/kg*	*Capacity= 4× 10-2 mol/kg*
$\equiv S^{s}OH$	*Capacity= 2 × 10-3 mol/kg*	*Capacity= 2 × 10-3 mol/kg*

Table B.2. Cation exchange reaction on planar sites and selectivity coefficients reported for Illite du Puy by (1) Bradbury and Baeyens (2009) and for Montmorillonite SWy-1 by (2) Bradbury and Baeyens (2017). (3) Value for Eu(III) as reported in Bradbury and Baeyens (2017), (4) value reported by Castellini et al. (2017), (3) value reported by Altmann et al. (2015)

	Ilite du Puy[1]	Montmorillonite Na-Swy-1[2]
$Na - Clay + H^+ \leftrightarrow H - Clay + Na^+$	*Log* K_c= 0.0	*Log* K_c= 0.0
$Na - Clay + K^+ \leftrightarrow K - Clay + Na^+$	*Log* K_c= 1.1	*Log* K_c= 0.48
$2Na - Clay + Mg^{2+} \leftrightarrow Mg - Clay + 2Na^+$	*Log* K_c= 1.04	*Log* K_c= 0.34
$2Na - Clay + Ca^{2+} \leftrightarrow Ca - Clay + 2Na^+$	*Log* K_c= 1.04	*Log* K_c= 0.61
$3Na - Clay + Al^{3+} \leftrightarrow Al - Clay + 3Na^+$	*Log* K_c= 1.0	*Log* K_c= 1.48[3]
CEC (meq/g)	*190[3]*	*870 / 661 [4]*

Table B.3. Sn(IV) hydrolysis constants

	Bradbury and Baeyens (2009)	Thermochimie V10a	NEA (Gamsjäger et al., 2012)
$Sn^{4+} + H_2O \leftrightarrow Sn(OH)^{3+} + H^+$	*log K* = 1.2		
$Sn^{4+} + 2H_2O \leftrightarrow Sn(OH)_2{}^{2+} + 2H^+$	*log K* = 1.7		
$Sn^{4+} + 3H_2O \leftrightarrow Sn(OH)_3{}^{+} + 3H^+$	*log K* = 1.6		
$Sn^{4+} + 4H_2O \leftrightarrow Sn(OH)_4 + 4H^+$	*log K* = 0.4	*log K* =7.54	
$Sn^{4+} + 5H_2O \leftrightarrow Sn(OH)_5{}^{-} + 5H^+$	*log K* = -7.7	*log K* =-1.06	
$Sn^{4+} + 6H_2O \leftrightarrow Sn(OH)_6{}^{2-} + 6H^+$	*log K* = -18.1	*log K* =-11.13	
$Sn(OH)_4 + H_2O \leftrightarrow Sn(OH)_5{}^{-} + H^+$			*log K* =-8.60 ± 0.40
$Sn(OH)_4 + 2H_2O \leftrightarrow Sn(OH)_6{}^{2-} + 2H^+$			*log K* =-18.67 ± 0.30

E Results of Blank sorption tests

The fraction of Sn lost is calculated such as:

$$Sn_{lost} = \frac{Sn_0 - Sn_{eq}}{Sn_0}$$

With Sn_0 (Bq/ mL), the concentration in the suspension before centrifugation using Equation (1) and Sn_{eq} (Bq/ mL), the concentration in the supernatant after centrifugation. Both concentrations are calculated based on the measured activities using Equation (1).

Type of experiments	solution	Equilibrium pH	Sn_0 ($\times 10^{-8}$ mol/L)	Sn_{eq} ($\times 10^{-8}$ mol/L)	Sn_{lost} (-)
Isotherm STx-1b	$NaClO_4$ 0.017 M	8.34	0.89	0.70	0.21
		8.40	0.93	0.85	0.09
		8.38	0.95	0.89	0.06
Effect S/L STx1-b		8.21	5.70	0.49	0.91
		8.22	5.79	0.47	0.92
		8.38	2.48	1.86	0.25
		8.41	3.58	3.68	-0.03
Isotherm IdP		8.46	2.00	1.87	0.06
		8.39	1.87	1.81	0.03
		8.48	1.92	1.84	0.04
Edge IdP		3.01	2.06	1.03	0.50
		6.96	6.20	0.23	0.62
		11.97	5.90	5.62	0.05
Edge _STx1-b		3.12	1.44	0.78	0.46
		6.95	1.61	0.79	0.51
		12.01	3.95	3.87	0.02
Isotherm STx-1b	$NaHCO_3$ 0.017 M	8.48	1.00	0.91	0.09
		8.45	0.97	0.90	0.08
		8.48	0.92	0.56	0.39
Isotherm IdP		8.51	3.07	3.00	0.02
		8.55	3.16	3.07	0.03
		8.55	3.02	2.99	0.01
Isotherm STx-1b	SSW	8.25	2.09	1.93	0.08
		8.28	2.09	2.02	0.03
		8.19	1.87	1.80	0.04
Isotherm IdP		8.39	3.70	1.92	0.48
		8.39	2.99	2.73	0.09
		8.34	3.31	2.66	0.20
Isotherm STx-1b	$NaClO_4$ 0.017 M + DOM_$NaClO_4$	8.40	6.70	6.07	0.09
		8.43	6.57	6.06	0.08
		8.41	0.63	0.59	0.07
Isotherm IdP		8.36	2.63	2.66	-0.01
		8.40	2.88	2.76	0.04
		8.38	2.88	2.82	0.02

F Uncertainty calculation for distribution coefficients K_d

The interaction constant is calculated such as:

$$K_d = \frac{CPM_0 - CPM_{eq}}{CPM_{eq}} \times \frac{V}{m} \quad (1)$$

And the corresponding uncertainty is calculated by propagating the experimental errors (confidence limit of 95 %) according to equation:

$$2\sigma(K_d) = K_d * \sqrt{\frac{2\sigma(CPM_0)^2 + \sigma\left(CPM_{eq}\right)^2}{\left(CPM_0 - CPM_{eq}\right)^2} + \frac{2\sigma\left(CPM_{eq}\right)^2}{\left(CPM_{eq}\right)^2} + \frac{2\sigma(V)^2}{(V)^2} + \frac{2\sigma(m)^2}{(m)^2}} \quad (2)$$

With

$$CPM_0 \; or \; CPM_{eq}\left(\frac{CPM}{mL}\right) = \frac{CPM_s - CPM_{bck}}{V_s} \quad (3)$$

And

$$2\sigma\left(CPM_0 \; or \; CPM_{eq}\right) = \left(CPM_0 \; or \; CPM_{eq}\right) * \sqrt{\frac{2\sigma(CPM_s)^2 + 2\sigma(CPM_{bck})^2}{(CPM_s - CPM_{bck})^2} + \frac{2\sigma(V_s)^2}{(V_s)^2}} \quad (4)$$

Where CPM_0 and CPM_{eq} are the specific counts of the suspensions and the supernatants, CPM_s and CPM_{bck} are the measured counts in LSC of the sample and the background, respectively, V and V_s, the total solution volume of the sorption experiments and the sample volume measured in LSC, respectively and m, the mass of clay in the sorption experiments. $2\sigma(V)/V=0.05$, $2\sigma(m)/m=0.05$ and the error of the sampled volume is assumed negligible, i.e $2\sigma(V_s)/V_s=0.0$

G XRD diffractograms of IdP and STx-1b

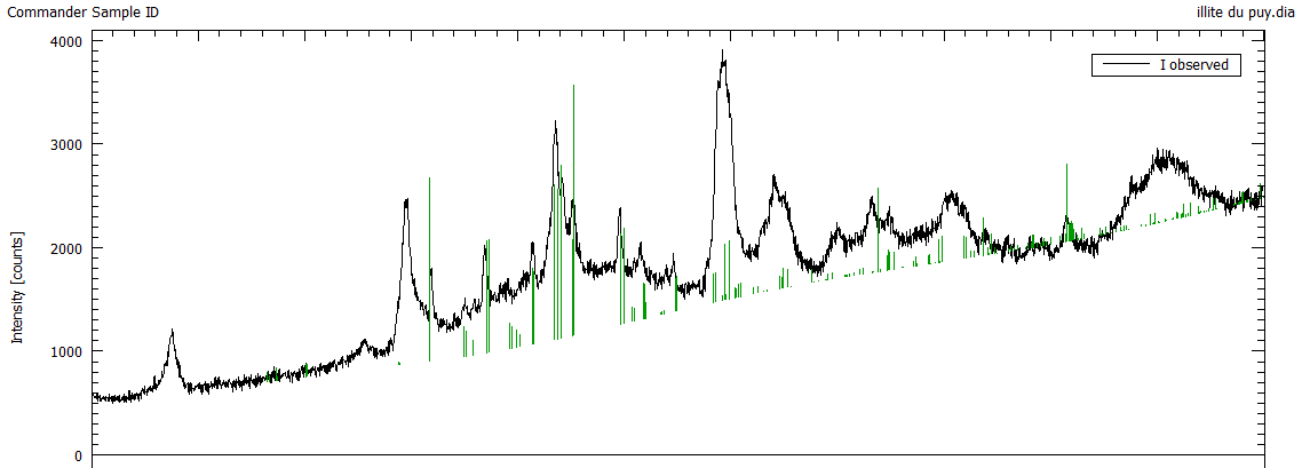

Figure G.1. XRD diffractogram of the used IdP

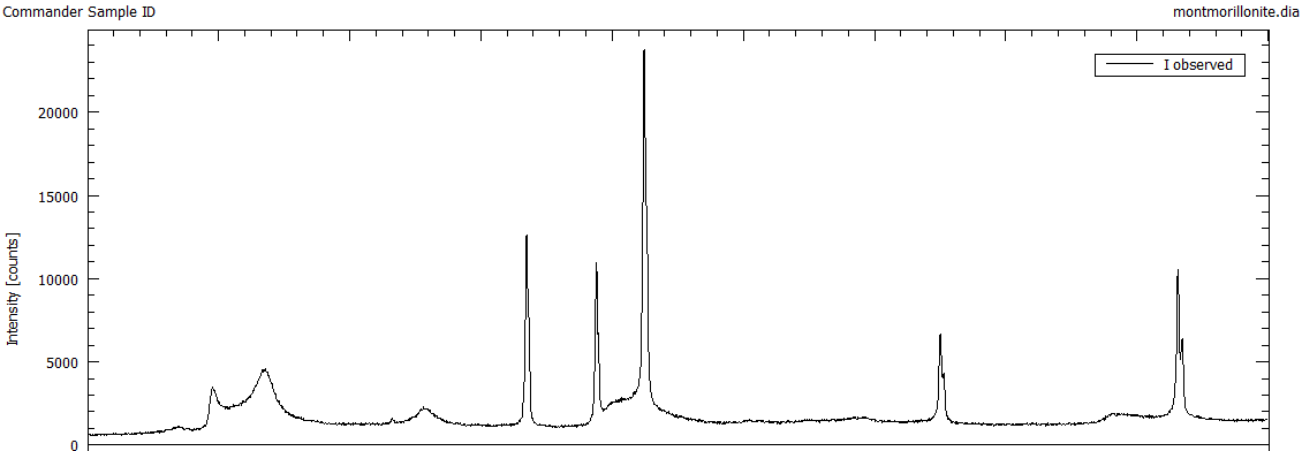

Figure G.2. XRD diffractogram of the used STx-1b montmorillonite